Perspective

Ferroelectric nematic liquid-crystalline phases

Nerea Sebastián,[1] Martin Čopič,[1,2] and Alenka Mertelj[1]
[1]*J. Stefan Institute, SI-1000 Ljubljana, Slovenia*
[2]*University of Ljubljana, Faculty of Mathematics and Physics, Ljubljana, Slovenia*

(Received 27 April 2022; published 17 August 2022)

Recent experimental realization of ferroelectric nematic liquid crystalline phases stimulated material development and numerous experimental studies of these phases, guided by their fundamental and applicative interest. In this Perspective, we give an overview of this emerging field by linking history and theoretical predictions to a general outlook of the development and properties of the materials exhibiting ferroelectric nematic phases. We will highlight the most relevant observations to date, e.g., giant dielectric permittivity values, polarization values an order of magnitude larger than in classical ferroelectric liquid crystals, and nonlinear optical coefficients comparable with several ferroelectric solid materials. Key observations of anchoring and electro-optic behavior will also be examined. The collected contributions lead to a final discussion on open challenges in materials development, theoretical description, experimental explorations, and possible applications of the ferroelectric phases.

DOI: 10.1103/PhysRevE.106.021001

I. INTRODUCTION

The term *liquid crystals* (LCs) refers to a state of matter, intermediate between isotropic liquid and solid state, whose properties fall in between. The liquid crystalline state is not unique, and there is a rich variety of phases, of which a given material can exhibit one or several. The least ordered of such phases is the nematic phase, in which the constituents exhibit long-range orientational order but no long-range translational order. The simple uniaxial nematic phase (N) formed by nonchiral molecules, is the most widely studied and technologically exploited of the liquid crystalline phases. On the other hand, chiral molecules are known to form a twisted (chiral) nematic phase (N*) and three so called blue phases characterized by a lattice of line defects. It has not been until the last decade that nematic phases have been added to this exclusive list. The twist-bend (TB) nematic phase (N_{TB}), predicted years before [1,2], was discovered [3–5] for achiral flexible dimer molecules. More recently, thermotropic polar nematic phases have been experimentally realized, which are the subject of this paper.

The idea that a nematic phase could be ferroelectric was suggested by Born more than a century ago [6]. In his paper, Born [6] proposed that experimentally observed phase transition from an isotropic to a nematic phase is a transition from a paraelectric to a ferroelectric phase and that such a phase transition can be described by a mean field theory analogous to the Langevin-Weiss theory for the phase transition from a paramagnetic to a ferromagnetic state. Decades later, Frank [7] discussed the consequence of polar order on elastic free energy density and realized that, in the case that the constituents of the nematic phase lack head-tail symmetry, polar order and splay deformation are connected. This was later studied in more detail by Pleiner and Brand [8], who showed that the phase exhibiting spontaneous splay deformation could be the thermodynamically stable ground state for some temperature interval. Palffy-Muhoray *et al.* [9] investigated the realizability of the ferroelectric nematic phase in terms of molecular constraints and concluded that, with careful molecular design, disk-shaped molecules can form a uniform nematic phase which is also ferroelectric. Using Monte Carlo simulations, Berardi *et al.* [10,11] showed that axially symmetric tapered, conical constituents with asymmetric interaction of the two ends can form polar phases even if they do not carry a dipole moment. Adding a small axial dipole results in a ferroelectric nematic phase. With increasing dipole moment, polar order starts to disappear, while simultaneously complex domain structures with local polar order arise [11].

In addition to all the theoretical analysis, experimentally, the ferroelectric nematic phase remained elusive for a long time. Polar order has been observed in some rigid linear polymers when they were sufficiently polymerized [12,13] and in a lyotropic cholesteric phase of poly L-glutamate [14]. Over a century after the Born paper, two types of low molecular mass materials exhibiting ferroelectric phases were reported. Nishikawa *et al.* [15] discovered that a material having a 1,3-dioxane unit in the mesogenic core, which they named DIO, exhibits three nematic phases. They showed that the lowest temperature phase exhibits polar arrangement of molecules, which results in large spontaneous electric polarization along the director [15]. Mandle *et al.* [16,17] designed a family of rodlike materials with a terminal nitro group and alkyloxy side group, which exhibits two nematic phases. The representative material of this family, RM734, was later studied in detail. It was shown by Mertelj *et al.* [18] and Sebastián *et al.* [19] that, at the phase transition between the nematic phases, simultaneously strong softening of splay deformation and growing ferroelectric order occur, resulting in a ferroelectric nematic order on the macroscopic scale. Chen *et al.* [20] then showed that the low-temperature phase has large ferroelectric domains

with saturated polarization of the same order of magnitude as the material DIO.

In this Perspective, we aim to give an overview of the recent experimental advances in the field of ferroelectric nematic LCs (NLCs) and frame them in the existing theoretical background. This Perspective is organized as follows. First, a brief description of nematic phases and comprehensive theoretical background is given. This is followed by a brief introduction of the most representative materials that exhibit polar nematic phases so far. Next, we expand on the experimental studies of polar phase, phase transitions, molecular dynamics (MD) simulations, and anchoring and electro-optic studies of ferroelectric nematic materials. Finally, we highlight the most important challenges to be treated in future research.

II. NEMATIC PHASES AND THEORETICAL BACKGROUND

A. Nematic phases

If we just focus on molecular LCs, they can be classically divided into thermotropic and lyotropic LCs. While the latter refers to materials in which the LC phase transitions occur by variation of the concentration of the LC molecules in a solvent (most commonly water), for thermotropic LCs, phases appear as a function of temperature. Although many different molecular structures form LC phases, they all share a common requirement which is an anisotropic molecular shape. Such an anisotropic shape will strongly determine the range of liquid crystalline phases exhibited by a material. There are multiple excellent texts covering the various liquid crystalline phases and their properties [21–24]. Here, we will exclusively focus on thermotropic nematic phases. For a long time, the range of known nematic phases was limited to a few, but the progressive investigation of molecular geometries has led to the discovery of a range of nematic mesophases. In this section, we shortly give a summary of them to establish the mesophase notation that will be followed throughout this Perspective (Fig. 1). Nonchiral rodlike molecules can exhibit a uniaxial nematic phase, which is homogeneous (N). The N phase possesses inversion symmetry and thus lacks polarity. The introduction of chirality in the rod molecules causes the director to twist in the chiral NLC (also known as cholesteric, N*). For odd LC dimers, the combination of molecular flexibility and bent shape leads to the so-called *TB nematic phase* (N_{TB}, Fig. 1), in which the director twists and bends in a heliconical structure. For bent molecules, also the splay counterpart, the so-called *splay-bend (SB) nematic phase* (N_{SB}, Fig. 1) has been predicted [1], involving a SB modulation. These will be treated in detail in the next section. For biaxial constituents, the biaxial nematic phase N_{bi} is predicted (Fig. 1) in which the directions perpendicular to the director are no longer degenerate. Despite the extended efforts, conclusive experimental discovery of the thermotropic biaxial nematic phase has been elusive so far [25–27].

The subject of this Perspective is the recently reported polar nematic phases, i.e., the ferroelectric nematic phase N_F, the ferroelectric chiral nematic phase N_F^*, and splay nematic N_S phases. The N_F phase, as in the case of the N phase, is uniaxial, but inversion symmetry is broken, and the phase is polar, with the polarization along the director. The introduction of the chirality leads in this case to N_F^* in which both the director and polarization twist along a helical axis (Fig. 1). On the other hand, N_S has been described as a modulated nematic structure, where splay deformation and polarization amplitude vary synchronously. Modulation can be one-dimensional (1D; Fig. 1) or two-dimensional (2D; see Fig. 1 in Ref. [28]).

Finally, it is worth noting here that thermotropic nematic materials can be combined with colloids to form interesting hybrid nematic systems with lower symmetry as, for example, biaxial [29], uniaxial, or biaxial ferromagnetic NLC [30,31], or those exhibiting reconfigurable monoclinic colloidal nematic order [32].

B. Macroscopic description

In this section, we will focus on several theoretical aspects required to build a macroscopic description of LC phases and relevant for the case of the ferroelectric nematic phases. Initially, a definition of the relevant order parameters is given, i.e., nematic order parameters, polarization, and shape polarity. Then Born's approach for the description between a paraelectric isotropic and a ferroelectric nematic phase is presented. Finally, the fundamentals of the Landau–de Gennes (LdG) approach for the description and analysis of phase transitions are given. A thorough introduction to order and phase transitions in soft materials, together with a comprehensive description of the Landau and LdG approaches to LCs can be found in Ref. [33]. Here, the description of the LdG theory is accompanied by its application in several examples, starting from the simplest isotropic-to-nematic phase transition and covering the different nematic-nematic transitions, from N-N_{TB} to the present cases of interest N-N_S and N-N_F.

1. Order parameters

An order parameter is defined as a physical quantity that is used to describe the order of a specific phase and is usually zero at the temperatures above the phase transition to that phase and has a finite value below it.

a. Order parameter of the nematic phase. At the phase transition from isotropic to usual uniaxial nematic phase, the second-rank tensor quantities, such as magnetic and electric susceptibilities, become anisotropic. Thus, the order parameter of such a uniaxial phase is a traceless second-rank tensor and can be written as $\mathbf{Q} = S(\mathbf{n} \otimes \mathbf{n} - \frac{1}{3}\mathbf{I})$. The unit vector $\mathbf{n}$, called the *director*, is oriented along the symmetry axis of the phase and has inversion symmetry $\mathbf{n} \equiv -\mathbf{n}$. Here, S is the magnitude of the order parameter describing how well the constituents are on average oriented along $\mathbf{n}$. The anisotropic parts of the magnetic and electric susceptibility tensors are proportional to S.

The anisotropic properties of the nematic phase are a consequence of the orientational order of constituents, e.g., molecules, which have anisotropic magnetic and electric polarizability tensors and/or are of anisotropic shape. In general, the orientation of a constituent is described by three Euler angles (α, β, γ), and the probability for a given orientation is described by the orientational distribution function (ODF) $f(\alpha, \beta, \gamma)$.

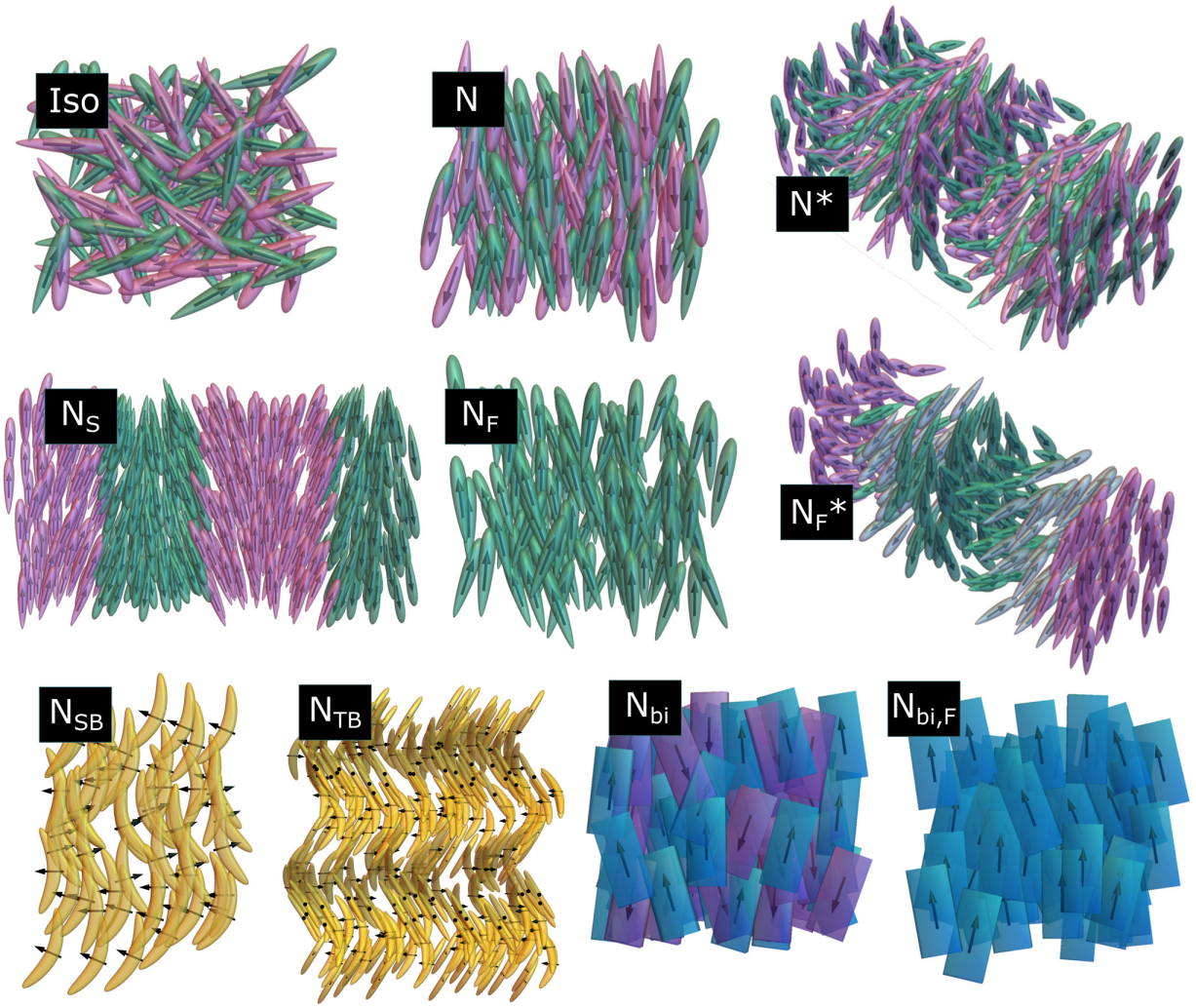

FIG. 1. Schematic representation of isotropic phase (Iso) and different nematic structures, where arrow represent electric dipole of the constituent: for polar-shaped molecules, nematic phase (N), chiral nematic or cholesteric phase (N*), splay nematic phase (N_S), ferroelectric nematic pahse (N_F), chiral ferroelectric phase (N_F^*), splay-bend nematic phase (N_{SB}), and twist-bend nematic phase (N_{TB}); for biaxial constituents, biaxial nematic phase (N_{bi}) and ferroelectric nematic phase ($N_{bi,F}$). Here, only cases with dipole moments along one symmetry axis are represented. In general, molecular dipole can be at an angle, which will contribute to the richness of possible phases, particularly in the case of biaxial nematics. Different colors are employed for the polar-shaped and biaxial constituents to indicate opposite dipole direction.

In the uniaxial case (symmetry C_∞), the ODF can be written as an even function of the cosine of the angle β between the axis of a constituent and **n**. The orientation of a molecule can be defined in more ways. The obvious choices are the normalized eigenvectors of one of the polarizability tensors or the normalized eigenvectors of the inertia tensor. As the eigensystems of these tensors are in general not the same, the magnitude of S calculated from the ODF as an average of the Legendre polynomial of the second-order P_2, $S = \langle P_2(\cos\beta)\rangle = \int f(\beta)P_2(\cos\beta)d(\cos\beta)$, will depend on this choice. This choice, however, will only determine the magnitude of the parameter S, while the terms and definitions of elastic constants remain the same.

In the case of a nonpolar biaxial nematic, the set of possible choices of the order parameter is larger [34]. The second-rank tensor physical quantities also become biaxial, and in general, their eigensystems do not need to coincide. Unlike in the uniaxial case, there is no obvious best choice of the order parameter. If the eigensystems of the second-rank tensors coincide, the biaxial symmetry is D_{2h}, or else it is lower.

b. Polarization. Polarization is defined as the volume density of molecular dipole moments and is a vector. Alternatively, the polar order can be described by a unit vector and an average of the Legendre polynomial of the first-order P_1, $\langle P_1\rangle = \langle\cos\beta\rangle = \int f(\beta)\cos\beta d(\cos\beta)$.

c. Shape polarity. Materials made of constituents that lack head-tail symmetry can in principle also form a polar nematic phase even if they do not carry dipole moments. In this case, the physical quantity which describes the orientation of the constituent is not a vector. The shape, described by the mass or volume distribution of a constituent, can be expressed by a series of multipoles (or if the shape is not rotationally symmetric, in a series of Wigner rotation matrices [35]), like as is common for a charge distribution. The only difference regarding the charges is that there is no negative mass, and consequently, a mass dipole is zero. Thus, the second nonzero

multipole is the mass quadrupole (described by the inertia tensor), which does not carry information about polarity. As already mentioned, it can be used for the description of the nonpolar nematic order. The lowest mass multipole that carries information about a head-tail nonsymmetric shape is described by an octupole T_{ijk}, and this can be contracted to a vector $P_i = T_{ijj}$.

2. Born approach

As mentioned, Born [6] proposed a mean field model to explain the transition between paraelectric isotropic and ferroelectric nematic phases. In this model, the ferroelectric phase emerges because of dipolar interactions between the constituents. The material is assumed to be a dipolar liquid composed of molecules with dipole moments $\mathbf{p}$. In an external electric field $\mathbf{E}_0$, a given molecule is exposed to a local field, which is a sum of the external field and the field resulting from the polar order of the surrounding molecules. This polar order is described as a volume density of dipole moments, i.e., polarization $\mathbf{P}$, and its contribution to the local field is proportional to it:

$$\mathbf{E}_{\mathrm{loc}} = \mathbf{E}_0 + \alpha \mathbf{P}. \tag{1}$$

The resulting torque on a dipole causes the molecules to tend to orient along the local field, which can be described in terms of the potential energy:

$$-\mathbf{p} \cdot \mathbf{E}_{\mathrm{loc}} = -pE_{\mathrm{loc}} \cos\beta. \tag{2}$$

In a liquid, a molecule, and with it the dipole, can rotate. When the field is applied, it still rotates, but on average, it is oriented along the local field for longer time. The probability for a given orientation is given by the Boltzmann distribution $1/A \exp[-\mathbf{p} \cdot \mathbf{E}_{\mathrm{loc}}/(k_{\mathrm{B}}T)]$, where A is the normalization constant, $A = \int \exp[-\mathbf{p} \cdot \mathbf{E}_{\mathrm{loc}}/(k_{\mathrm{B}}T)] d\Omega$, and integration is performed over a solid angle Ω. The magnitude of $\mathbf{P}$ can then be written as an average:

$$P = \rho_N p \langle \cos\beta \rangle, \tag{3}$$

where ρ_N is the number density, $\rho_N = \frac{N}{V}$. By defining $T_0 = \rho_N \alpha p^2/(3k_{\mathrm{B}})$ and $x = \alpha p P/(k_{\mathrm{B}}T)$, Eq. (3) becomes

$$\frac{T}{3T_0} x = L(x), \tag{4}$$

where $L(x)$ is the Langevin function, $L(x) = \coth(x) - 1/x$. This equation gives a real solution for x when the temperature T is lower than T_0. Thus, this model predicts that, at T_0, the system undergoes the transition to the polar phase, and below this temperature, it exhibits spontaneous polarization $P = k_{\mathrm{B}}T x_T/(\alpha p)$, where x_T is the solution of Eq. (4) at temperature T.

In Eq. (1), the contribution $\alpha\mathbf{P}$ to the local field is a sum of the dipolar fields of the surrounding molecules. In the mean field approach, α is the depolarization factor, which for a spherical cavity is equal to $1/(3\varepsilon_0)$. This is the value that Born took. However, the magnitude of the dipolar field decreases as r^{-3}; thus, on a given molecule, the nearest neighbors are those that contribute the most to the field. Moreover, because of the anisotropy of the dipolar field, the local field will strongly depend on the relative positions and orientations of the neighbors. In magnetic dipolar liquids, the simple mean field approach has been shown to overestimate the local field, and the question of whether the dipolar interaction alone can lead to polar order remained unanswered [36]. On the other hand, the shape of the constituents can strongly affect the positional and orientational correlations between neighbors, and thus, it can promote or prevent the formation of the polar phase. A dipolar liquid made of platelike constituents is more likely to exhibit a polar nematic phase than the one made of rods [9,37].

Finally, it is important to remark here that, considering the current understanding, the polar nematic phases discussed in this Perspective are not the phases predicted by the Born model. This will be further elaborated in Sec. IV C.

3. LdG approach

A general and very useful way to describe and analyze phase transitions (and general field dynamics) is via the LdG (in the general context Landau-Ginzburg) approach [38–40]. It consists of writing the free energy of a system in the high-symmetry phase in terms of a characteristic quantity, the order parameter. Such a characteristic quantity is usually defined to be zero in the high-symmetry phase and nonzero in the low-symmetry phase. The free energy must be constructed in terms of the invariants (scalars) of the order parameter with respect to the high-symmetry phase. The equilibrium state is then found by minimization of the free energy with respect to the order parameter.

Often there are other quantities that also appear in the low-symmetry phase and are of interest. Such quantities are called secondary order parameters. The LdG free energy then contains their invariants and the invariant coupling terms with the primary order parameter. To treat the possible deformations of the phase and to include the possibility of spatially modulated phases, gradient terms must be added to the free energy F.

Let us first briefly look at the basic LdG F for the transition from the isotropic (I) to the nematic (N) phase, as there are some issues that will be relevant for the properties of the polar N phases. The free energy density is [38]

$$\begin{aligned} f = {} & \tfrac{1}{2}A\mathbf{Q}^2 + \tfrac{1}{3}B\mathbf{Q}^3 + \tfrac{1}{4}C\mathbf{Q}^4 \\ & + \tfrac{1}{2}L_1 Q_{ij,k} Q_{ij,k} + \tfrac{1}{2}L_2 Q_{ij,j} Q_{ik,k}. \end{aligned} \tag{5}$$

Here, $Q_{ij,k} = \partial Q_{ij}/\partial x_k$. The quadratic coefficient A is assumed to become negative at some temperature T_{c} and so drives the transition. The cubic B term causes the transition to be first order. Here, B is also important in another respect. When $B = 0$, the low-temperature order is degenerate. The minimum of f occurs for a manifold of states from oblate uniaxial with $S < 0$ to prolate uniaxial with $S > 0$ and biaxial states in between. If $B < 0$, the N phase is prolate uniaxial (usual calamitic N), and with $B > 0$, the low phase is oblate uniaxial (molecules are on average perpendicular to an axis but disordered in the plane). Therefore, the B term forces the uniaxial state with an effective potential $|BS|\ p_b^2$, where p_b is the degree of biaxial order. The empirical values for B are quite large [41]. For example, a bend deformation by symmetry induces local biaxiality. By taking the value of B from Ref. [41] and calculating p_b in a hybrid cell (with planar

boundary conditions on one surface and homeotropic on the other), we get that biaxiality becomes appreciable only when the bend radius is of the order of 1 nm.

The second point concerns the elastic terms L_1 and L_2. The elastic energy of a nematic is usually written in terms of the director. It has the form proposed by Frank and Oseen [7,42]:

$$f_N = \tfrac{1}{2}\{K_1(\nabla\cdot\mathbf{n})^2 + K_2[\mathbf{n}\cdot(\nabla\times\mathbf{n})]^2 + K_3[\mathbf{n}\times(\nabla\times\mathbf{n})]^2\}. \quad (6)$$

The first term is the splay deformation, in which the director diverges or converges, the second is the twist (perpendicular to the director), and the third term corresponds to the bend deformation. The Frank-Oseen elastic energy contains three elastic constants: splay (K_1), twist (K_2), and bend (K_3). In terms of L_1 and L_2, $K_1 = K_3$. This degeneracy is broken by higher-order terms of the form $\mathbf{Q}(\nabla\mathbf{Q})^2$ [43,44].

We also need to consider the polarization vector $\mathbf{P}$. This does not need to be electric polarization but can also be steric, describing, for example, pear-shaped molecules. Polarization brings terms to the free energy including the couplings to the nematic order. The lowest term $\mathbf{P}\cdot\mathbf{Q}\cdot\mathbf{P}$ forces $\mathbf{P}$ to be parallel to the largest or smallest eigenvector of $\mathbf{Q}$. In the usual uniaxial case, this means that $\mathbf{P}$ is either parallel or perpendicular to $\mathbf{n}$, depending on the sign of the term.

The second very important terms are the so-called *flexoelectric couplings* of $\mathbf{P}$ to $\nabla\mathbf{Q}$. Their importance was recognized by Frank [7] and later by Meyer [45], who also recognized that flexoelectricity can lead to instabilities. In terms of the director, there are two such terms: splay $e_1\mathbf{n}(\nabla\cdot\mathbf{n})\cdot\mathbf{P}$ and bend $e_3(\mathbf{n}\times\nabla\times\mathbf{n})\cdot\mathbf{P}$. To the lowest order in $\mathbf{Q}$, there is just one flexoelectric term $(\nabla\cdot\mathbf{Q})\cdot\mathbf{P}$. Thus, as in the case of elastic constants, the flexoelectric coefficients are also degenerate to this order. This degeneracy is then broken by terms of the form $P_iQ_{ij}Q_{jk,k}$ ($\mathbf{P}\cdot\mathbf{Q}\cdot\nabla\cdot\mathbf{Q}$). We note here that flexoelectric coupling, together with the term $\mathbf{P}\cdot\mathbf{Q}\cdot\mathbf{P}$, also breaks the degeneracy of K_1 and K_3.

Considering a polar nematic phase, one can take just $\mathbf{P}$ as the primary order parameter. This was done by Pleiner and Brand [8]. They wrote the free energy density in the form:

$$f = -\tfrac{1}{2}a\mathbf{P}^2 + \tfrac{1}{4}b\mathbf{P}^4 - c_0\nabla\cdot\mathbf{P} + \tfrac{1}{2}c_1(\nabla\cdot\mathbf{P})^2 + \tfrac{1}{2}c_2(\nabla\times\mathbf{P})^2. \quad (7)$$

As $\mathbf{P}$ is a polar vector, the term c_0 div $\mathbf{P}$, which is linear in splay deformation, is allowed and leads to a structure with spontaneous splay. Since it is impossible to fill the space with homogeneous splay, the authors discussed possible structures that included defects.

a. N_{TB} *and* N_{SB} *phases.* With a free energy in terms of $\mathbf{n}$, including second-order gradient terms, Dozov [1] considered the case where the bend elastic constant K_3 would become negative so that the homogeneous N phase becomes unstable. As homogenous bend also cannot fill the space, the new phase can exhibit either TB (N_{TB}) or SB (N_{SB}) modulation (Fig. 1), depending on the ratio K_1/K_3. The N_{TB} phase was indeed found by Cestari *et al.* [3], Borshch *et al.* [5] and Chen *et al.* [4]. In Ref. [46], it was also shown by light scattering that indeed K_3 becomes very small close to the transition.

Following the observation of Meyer [45] that a bend must be accompanied by flexoelectric polarization, Shamid *et al.* [47] proposed a model for the transition from N to the N_{TB} phase. They started with a free energy density:

$$f = \tfrac{1}{2}K_1\mathbf{S}^2 + \tfrac{1}{2}K_2T_{tw}^2 + \tfrac{1}{2}K_3\mathbf{B}^2 + \tfrac{1}{2}\mu\mathbf{P}^2 - \lambda\mathbf{B}\cdot\mathbf{P} + \tfrac{1}{4}\nu\mathbf{P}^4 + \tfrac{1}{2}\kappa(\nabla\mathbf{P})^2, \quad (8)$$

where $\mathbf{S}$, T_{tw}, and $\mathbf{B}$ denote the splay, twist, and bend deformations. The flexoelectric coupling renormalizes the bend elastic constant to $K_{3\text{eff}} = K_3 - \lambda^2/\mu$. This shows that the measured $K_{3\text{eff}}$ can become zero due to either decreasing K_3 (bare elastic constant) or μ. In Ref. [47], μ is taken to be temperature dependent, so $\mathbf{P}$ is the primary order parameter and drives the transition. In the N_{TB} phase, $\mathbf{P}$ forms a helical structure, and thus, the N_{TB} can also be considered a ferrielectrical phase. Their paper [47] also finds the same conditions as Dozov [1] for either N_{TB} or N_{SB} to be stable. Additionally, it presents numerical simulation results of a lattice model that also shows a periodic TB or SB structure.

Shamid *et al.* [48] looked at the possibility that polarity of the N phase would result in hexagonal or cubic periodic structures with twist and bend, in an analogous way to the chirality-induced blue phases. In addition to a numerical lattice calculation, they present an LdG analysis based on the free energy:

$$f = \tfrac{1}{2}A\mathbf{Q}^2 + \tfrac{1}{3}B\mathbf{Q}^3 + \tfrac{1}{4}C\mathbf{Q}^4 + \tfrac{1}{2}L_1Q_{ij,k}Q_{ij,k} + \tfrac{1}{2}L_2Q_{ij,j}Q_{ik,k} + \tfrac{1}{2}\mu\mathbf{P}^2 + \tfrac{1}{4}\nu\mathbf{P}^4 + \tfrac{1}{2}\kappa(\nabla\mathbf{P})^2 + \lambda\mathbf{P}\cdot(\nabla\cdot\mathbf{Q}) + \eta\mathbf{P}\cdot\mathbf{Q}\cdot\mathbf{P}, \quad (9)$$

where $\mathbf{Q}$ and $\mathbf{P}$ are expanded in the lowest-order Fourier modes. The model predicts, in addition to I, N, and N_{TB} phases, a stable cubic body-centered cubic and a 2D hexagonal phase consisting of a lattice of defects. The latter phases have not been observed yet.

Longa and Pająk [49] analyzed the possible 1D periodic structures by including both $\mathbf{P}$ and intrinsic chirality. To Eq. (9), they added a chiral term $\mathbf{Q}\cdot(\nabla\times\mathbf{Q})$, which generates the N^* phase, and a chiral coupling $(\nabla\cdot\mathbf{Q})\cdot(\nabla\times\mathbf{P})$. This last term is not allowed for electrical polarization but is possible for steric dipoles. Two fourth-order terms were also added. With all terms, six possible structures were found including the usual N^* phase. All phases except N^* also have periodically modulated $\mathbf{P}$ and biaxiality. The N_S phase is not among those structures. In both papers [48,49], K_1 and K_3 are degenerate, and the N_{TB} phase is obtained by the positive $\mathbf{P}\cdot\mathbf{Q}\cdot\mathbf{P}$ term favoring the bend flexopolarization ($\mathbf{n}$ perpendicular to $\mathbf{P}$).

b. N_S *and* N_F *phases.* We now move to the main theme of this Perspective, which is the splay N_S (Fig. 1) and the homogenous ferroelectric N_F phase (Fig. 1). In Ref. [18], it was shown by dynamic light scattering that, in the upper N phase of RM734, the splay constant K_1 becomes very small before the transition to the N_S phase. The transition is modeled by a free energy:

$$f = \tfrac{1}{2}L_1Q_{ij,k}Q_{ij,k} - L_5Q_{ij}Q_{ik,k}Q_{jl,l} - \gamma P_iQ_{ij,j} + \tfrac{1}{2}t\mathbf{P}^2 + \tfrac{1}{2}b(\nabla\mathbf{P})^2. \quad (10)$$

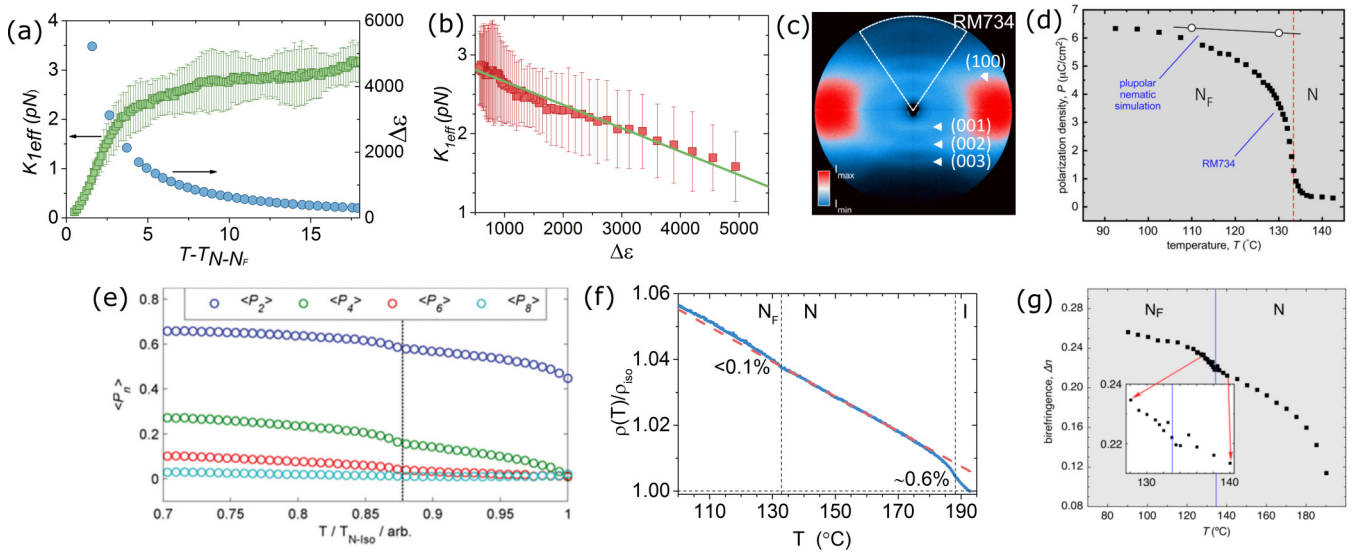

FIG. 2. (a) Temperature dependence of the effective splay elastic constant ($K_{1,\mathrm{eff}}$) and amplitude of the main dielectric relaxation mode in the N phase of RM734 ($\Delta\varepsilon_{\mathrm{low}}$). (b) $K_{1,\mathrm{eff}}$ vs interpolated values of $\Delta\varepsilon_{\mathrm{low}}$ showing linear dependence. (a) and (b) © 2020 American Physical Society. Reproduced with permission from Ref. [19]. (c) Magnetically aligned two-dimensional x-ray scattering pattern in the N phase of RM734. Reproduced from Ref. [71], licensed under CC BY 4.0. (d) Temperature dependence of the electric polarization P. Reproduced from Ref. [20], licensed under CC BY 4.0. (e) Temperature dependence of the first four even-order parameters. Reproduced from Ref. [77], licensed under CC BY 4.0. (f) Measured temperature dependence of the normalized density, where dashed lines is the extrapolated value from the N phase. Reproduced from Ref. [71], licensed under CC BY 4.0. (g) Temperature dependence across the N and N_F phase of the birefringence. Reproduced from Ref. [20], licensed under CC BY 4.0.

This is the simplest elastic energy where $K_1 = L_1S^2 - \frac{2}{3}L_5S^3$ and $K_3 = L_1S^2 + \frac{4}{3}L_5S^3$ are not degenerate. The term $(\mathbf{\nabla P})^2$ is necessary to stabilize the splayed state. Assuming uniaxial symmetry, the results are analogous to those in Ref. [47]. The transition to N_S occurs when $K_{1\mathrm{eff}} = L_1S^2 - \frac{2}{3}L_5S^3 - \gamma^2/t = 0$. The bend constant is also renormalized: $K_{3\mathrm{eff}} = L_1S^2 + \frac{4}{3}L_5S^3 - \gamma^2/t$, but if $L_5 > 0$, splay becomes unstable first. The instability can be driven either by decreasing bare K_1 due to the dependence on S or by decreasing t, that is, by the ordering of $\mathbf{P}$. The form of the T dependence of $K_{1\mathrm{eff}}$, shown in Fig. 2(a), where $K_{1\mathrm{eff}}$ is only slowly decreasing to ~5 K above the transition and then rapidly goes to 0, is consistent with t driving the transition. The model in Eq. (5) also predicts that, close below the transition temperature $t_c = \gamma^2/K_1$, the amplitude of the splay angle and the modulation wave vector are proportional to $\sqrt{t_c - t}$ and $\mathbf{P}$ to $(t_c - t)$.

In Ref. [18], it is also pointed out that, if $L_5 < 0$, the free energy in Eq. (5) predicts the N_{TB} phase. This is further elaborated in Ref. [50]. The unified treatment of N_S and N_{TB} phases is one of the advantages of using the tensor order parameter $\mathbf{Q}$ to construct the free energy. The dependence of the L_5 term on S^3 could also be important in driving the N_{TB} transition, as suggested in Fig. 2 of Ref. [50]. By parametrizing $\mathbf{Q}$ as a biaxial tensor, Eq. (10) would also give the amount of local biaxiality due to splay or bend. In that case, it is necessary to include the $B\mathbf{Q}^3$ term, as discussed above and done in Ref. [49].

Chaturvedi and Kamien [51] analyzed the mechanisms for the transition to the modulated N phases in terms of $\mathbf{n}$. They tried bond orientational ordering and found that, in the lowest order, it does not lead to the modulated phases. They conclude that the flexoelectric coupling is the important mechanism and consider the symmetry of the N_{SB} and N_S phases on exchanging bend and splay flexoelectric coupling.

The periodicity of the splay in N_S can also be 2D. This was pointed out by Rosseto and Selinger [28]. They considered the free energy in Eq. (9) and expanded it to fourth order in all variables. They found that doubly periodic splay has slightly lower energy except very close to the N_S transition and $K_1/K_3 > 3$. They also found that, at a scaled temperature sufficiently below the transition, the homogeneous ferroelectric phase N_F is the stable one.

The stability of the N_F phase was also studied by Kats [52]. He takes free energy with $\mathbf{P}$ as the primary parameter:

$$f = \tfrac{1}{2}t\mathbf{P}^2 + \tfrac{1}{4}\lambda\mathbf{P}^4 + \tfrac{1}{2}b(\mathbf{\nabla P})^2 + \beta_1\mathbf{P}^2(\mathbf{\nabla}\cdot\mathbf{P}) + \beta_2(\mathbf{P}\cdot\mathbf{\nabla})\mathbf{P}^2 + \tfrac{1}{2}K(\mathbf{\nabla n})^2 + \gamma(\mathbf{P}\cdot\mathbf{n})^2 + e_1\mathbf{P}\cdot\mathbf{n}(\mathbf{\nabla}\cdot\mathbf{n}) + e_2\mathbf{P}\cdot(\mathbf{n}\cdot\mathbf{\nabla})\mathbf{n}, \quad (11)$$

where one nematic elastic constant approximation is used. Flexodipolar terms of $\mathbf{P}$ coupled to $\mathbf{\nabla P}$ are also added. Depending on the sign of γ, $\mathbf{P}$ is either perpendicular ($\gamma > 0$) or parallel ($\gamma < 0$) to $\mathbf{n}$. In both cases, the condition of stability is derived by considering small perturbations of the ground state. In the perpendicular case, it is found that N_F is stable if the flexodipolar interaction is neglected ($\beta = 0$). In the parallel case (the experimentally observed N_F), the stability criterion is somewhat complicated and depends on all the parameters. The instability occurs for the 1D and 2D periodic perturbation at the same point in parameter space.

In discussing the stability of the homogeneous N_F phase, it is necessary to note a paper by Khachaturyan [53]. In this paper, the author considers the electrostatic self-energy of **P**, which is not included in the models above. The result points out that a ferroelectric fluid is unstable against a twist with an axis perpendicular to **P**, analogous to the N^* phase.

4. Electrostatics

In the description of ferroelectric material, there is an additional contribution to the energy of the system due to the so-called *depolarization field*, which is the field created by the spontaneous electric polarization. In the absence of free charges and external field, it can be calculated using Gauss's law $\nabla \cdot \mathbf{D} = \nabla \cdot (\varepsilon_0 \boldsymbol{\varepsilon} \mathbf{E}_{\text{dep}} + \mathbf{P}) = 0$, where $\boldsymbol{\varepsilon}$ is a dielectric tensor. Effectively, this means that the depolarization field $\mathbf{E}_{\text{dep}}$ is generated by bound charges generated by $-\nabla \cdot \mathbf{P}$. For a finite piece of material, they can be divided into surface charge $\sigma_b = \nu \cdot \mathbf{P}$, where $\boldsymbol{\nu}$ is normal to the surface, and volume charge $\rho_b = -\nabla \cdot \mathbf{P}$. These charges are sources of electrostatic potential from which $\mathbf{E}_{\text{dep}}$ is calculated. The contribution of the depolarization field to free energy is

$$F_{\text{dep}} = -\frac{1}{2}\int_V \mathbf{E}_{\text{dep}} \cdot \mathbf{P} dV, \tag{12}$$

where integration is performed over the ferroelectric body. As the ferroelectric NLCs exhibit large polarization values, this contribution to the total free energy is important. In the general case, the calculation of the structure affected by the depolarization field is challenging. However, if **P** is parallel to **n**, i.e., $\mathbf{P} = P\mathbf{n}$, and it depends only on one Cartesian coordinate (let us say z), for example, when in a thin layer oriented perpendicularly to z and confined by nonconducting boundaries, then the depolarization field energy becomes

$$F_{\text{dep}} = \frac{1}{2}A\int_0^d \frac{n_z^2(z)P^2(z)}{\varepsilon_0\left[\Delta\varepsilon n_z^2(z) + \varepsilon_\perp\right]} dz, \tag{13}$$

where n_z is the z component of **n**, $\Delta\varepsilon = \varepsilon_\parallel - \varepsilon_\perp$ with $\varepsilon_\parallel$ and $\varepsilon_\perp$ being the components of $\boldsymbol{\varepsilon}$ parallel and perpendicular to **n**, and A the surface of the layer. From Eq. (13), it follows that the depolarization energy favors that **P** lays in the plane of the layer and that the field of the order of $E_{\text{ext}} \approx P/(\varepsilon\varepsilon_0)$ is needed to orient **P** perpendicularly to the layer. Similarly, when the system exhibits 1D modulated splay structure, the integrand in Eq. (13) can be added as a new term to the free energy density in Eq. (10). For small splay modulations, for example, at the phase transition from N to N_S phase, this term only slightly rescales the $\mathbf{P}^2$ term and causes a small reduction of t_c.

In a general case, when **P** (and **n**) depends on more coordinates, the material is surrounded by conducting homogenous or patterned surface, e.g., electrodes, and/or the ions are present, the combined LdG and Poisson-Boltzmann theoretical framework (e.g., as in Refs. [54,55]) should be used for the studies of possible structures.

C. Difference with other polar liquid crystalline mesophases

It is important to recall here the differences between the ferroelectric nematic phases subject of this Perspective and classical ferroelectric LCs. Here, we are dealing with LC phases without any degree of positional ordering. In the LC community, the nomenclature ferroelectric LCs was historically employed to address tilted layered mesophases shown by chiral mesogens (SmC*), in which molecules are tilted with respect to the layer normal and due to the molecular chirality; such a tilt turns from layer to layer, forming a helix. As pointed out by Meyer *et al.* [56], if there is a component of the molecular dipole perpendicular to the molecular long axis, symmetry allows the existence of spontaneous polarization in the direction perpendicular to the tilt plane. As the tilt plane turns around the layer normal from layer to layer, the direction of the layer polarization also makes the same turn. Although the SmC* is truly defined as helielectric, it is usually labeled as ferroelectric because of the ferroelectric phase generated by unwinding the helix. Opposite tilts in adjacent layers give rise to the antiferroelectric counterpart SmC_A^*. Nice reviews about classical ferroelectric mesophases can be found in Refs. [57–59].

Niori *et al.* [60] described a system of polar mesophases formed by nonchiral rigid bent-core molecules, where the layer normal, the tilt direction, and the layer polarity define a system which is either left- or right-handed. Then the bent-core molecules can develop chiral structures and with them polar phases, despite being achiral. In contrast to polar phases exhibited by calamitics, in bent-core molecules, polarization and tilt are no longer correlated. A change of the tilt or polarization direction implies the inversion of the layer chirality. Numerous layered polar structures have been described for bent-core molecules for which nice reviews can be found in Refs. [25,61,62].

Also worth mentioning are efforts devoted to promoting polar columnar phases, consisting of disk-shaped molecules in which molecules stack to form columns [63–65], showing polar order with polarization along the columns. For a detailed review of such phases, readers can refer to Ref. [66].

This section does not aim to be an in-depth review of ferroelectricity in liquid crystalline phases but to highlight the differences with respect to the recently described polar nematic phases. The different systems described in this section possess some degree of long-range positional order as a requisite for the appearance of polar ordering. However, as pointed out before, polar nematic phases are unique in that only long-range orientational order is present and three-dimensional fluidity is retained.

III. MATERIALS

In this section, the materials which have been shown to exhibit ferroelectric nematic phases so far will be briefly presented.

In Fig. 3, three representative materials exhibiting the ferroelectric nematic phase are shown. All three have a large longitudinal dipole moment component. DIO and the material **1** from Ref. [67] belong to fluorinated nematogen materials, which are widely used in LC displays [68]. Although these kinds of materials have been extensively studied in the past, so far, materials like DIO that show the ferroelectric nematic phase are scarce [69]. On the contrary, Mandle *et al,* [16,17] showed that several materials like RM734 exhibit two nematic

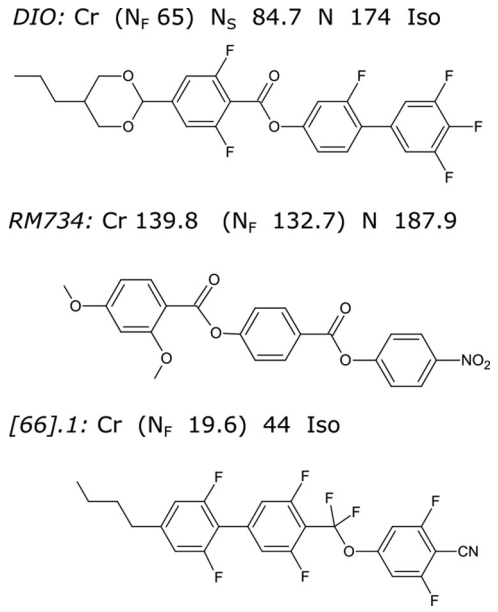

FIG. 3. Chemical structure of three representative materials exhibiting ferroelectric nematic phase and their phase sequences.

phases. In addition to large longitudinal dipole moment, these materials have a terminal nitro group and lateral alkyloxy group. With the appearance of lower temperature, ferroelectric nematic phase is strongly sensitive to small structural changes, e.g., replacing the terminal nitro group with another dipole group; removal of a single ester unit or the lateral group from RM734 prevents its formation [16,70]. On the other hand, moving the lateral group to the middle ring or fluorination of any of the rings affects the phase transition temperatures and, in some cases, increases the ferroelectric polarization [16,69,71]. The obvious question is then: What molecular features are favorable for the appearance and stability of the polar nematic phases? Li *et al.* [69] reported a series of molecules starting from close derivatives of DIO and RM734 and subsequently shortening or lengthening the molecules, introducing ester, fluoride, fluorocarbon ether, nitro, nitrile, or trifluorocarbon groups as electron-withdrawing groups to control the molecular dipole moment. Materials are then classified according to the exhibition of stable, metastable, or absent polar nematic phase. The authors conclude that, statistically, the most critical parameter is the magnitude of the molecular dipole moment ($\mu > 9$ D).

The third molecule represented in Fig. 3, material **1** from Manabe *et al.* [67], contains fluorinated biphenyl and phenyl units bridged by a difluoromethoxy group and is terminated by a nitrile group [67]. Note that, contrary to RM734 and homologues, the nitrile group does not hinder in this case the appearance of the polar phase. The calculated dipole moment adds up to ∼11.3 D. Remarkably, material **1** from Ref. [67] shows direct Iso-N$_F$ transition, being the ferroelectric phase accessible at temperatures slightly below room temperature. It is speculated that the relatively long butyl chain is responsible in this case for the low temperatures.

The polar phase in low molecular weight RM734-like materials has been shown to also extend to rigid oligomers by Li *et al.* [72] and polymers by Li *et al.* [69] and Dai *et al.*

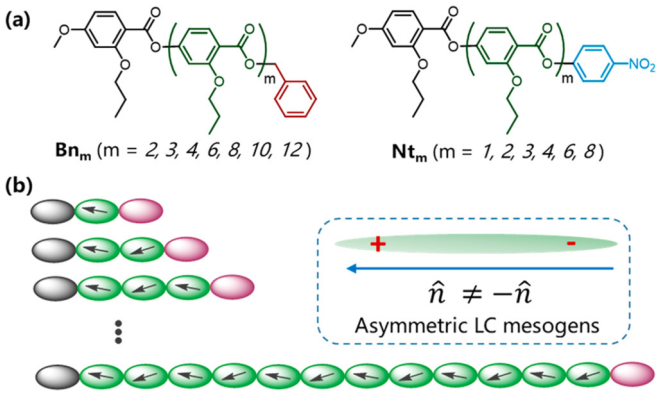

FIG. 4. Oligomers. (a) Chemical structure of Bn$_m$ and Nt$_m$ main-chain liquid crystal (LC) oligomers. (b) Schematic representation of the mesogens. © 2021, American Chemical Society. Reprinted with permission from Ref. [72].

[73]. Oligomers made of repeating p-oxybenzoate units with the propoxy side group (Fig. 4) have dipole moments which increase with the number of repeated units and can reach values >30 D. Most of them exhibit a direct transition from isotropic to ferroelectric nematic phase [72], with transitional temperatures shifting up with the increase of the oligomer length.

On the other hand, Li *et al.* [69] and Dai e*t al.* [73] studied three side-chain LC polymers based on RM734 and showed that LC polymers with RM734-like mesogen side-joined (Fig. 5) to form the polar phase, while the polymers with end-jointed mesogens self-assemble into a smectic A phase with no polarity. They also showed that the magnitude of the dipole moment of the side mesogen is critical for the appearance of macroscopic polarity in these liquid crystalline polymers. In this case, transition temperatures are also quite above room temperature, with melting temperatures >100 °C.

As shown in this chapter, despite the early stages of the research, in the past few years, several materials showing the polar nematic phases have slowly accumulated.

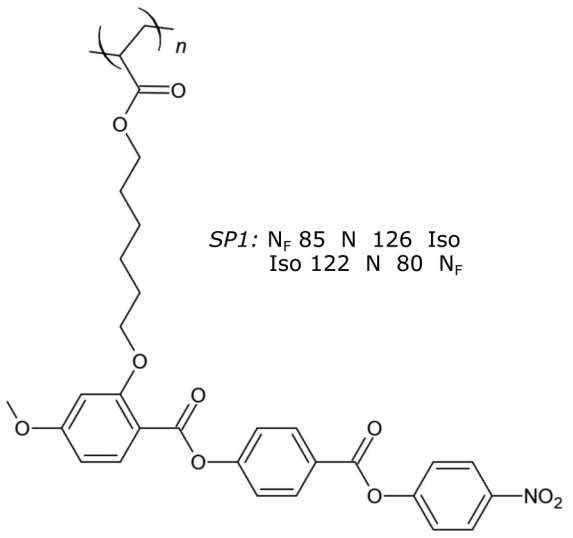

FIG. 5. Chemical structure of the SP1 side-chain liquid crystalline polymer and its phase sequence on heating and cooling [73].

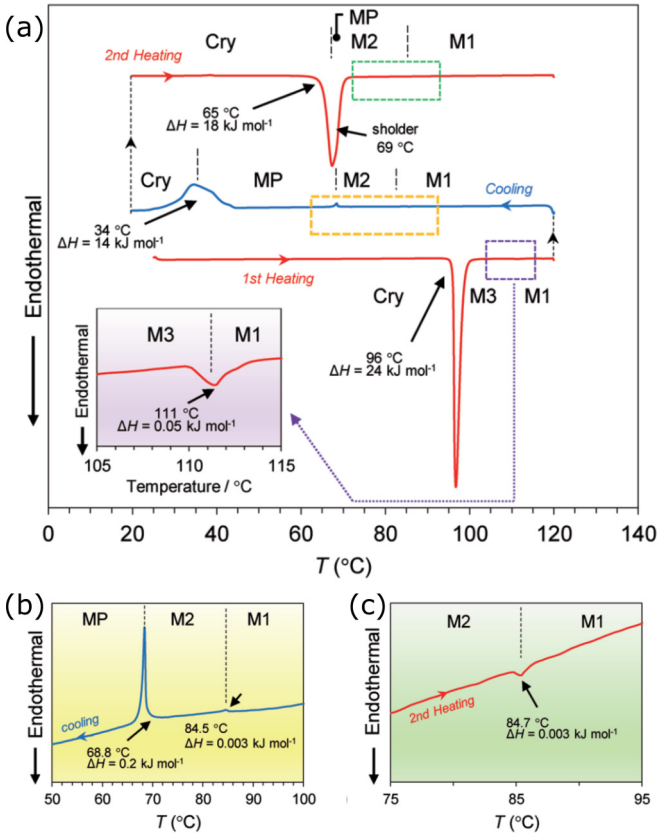

FIG. 6. Differential scanning calorimetry (DSC) curves of DIO at 5.0 K/min for heating and cooling scans. (a) First heating scan (bottom) and subsequent cooling and heating runs. (b) Zoom-in detail of M1-M2 (N-N_S) and M2-MP (N_S-N_F) transitions on cooling. (c) A close look at the M2-M1 (N_S-N) transition during second heating. © 2017 WILEY-VCH Verlag GmbH & Co. KGaA, Weinheim. Reprinted with permission from Ref. [15].

IV. POLAR PHASES AND PHASE TRANSITIONS

In this section, the most significant current experimental findings will be covered. An introduction of methods and their challenges in the frame of research on ferroelectric nematic materials will be presented in Sec. VI.

A. Nonchiral phases and phase transitions

As mentioned above, three distinct nematic phases were originally reported for DIO by Nishikawa *et al.* [15]. On cooling from the higher-temperature mesophases, the differential scanning calorimetry (DSC) curve reveals two exothermic peaks at 84.5 °C ($\Delta H = 0.003\,\mathrm{kJ\,mol^{-1}}$) and 68.8 °C ($\Delta H = 0.2\,\mathrm{kJ\,mol^{-1}}$), evidencing two weak first-order transitions between three mesophases (see Fig. 6). As will be discussed below, those phases can be identified from high to low temperature as N (M1), N_S (M2), and N_F (MP). The nomenclature N, N_S, and N_F will be used from now on for clarity. The identification of M2 as N_S to designate the intermediate phase found in DIO will be discussed in detail in Sec. VI. It is worth recalling here the much weaker character of the N-N_S transition than the N_S-N_F one. Further cooling results in the crystallization of the sample at 34 °C.

The same year, Mandle *et al.* [16] reported for RM734 (Compound 2 in Ref. [16]) the phase sequence Cr 139.8 °C (N_x 132.7 °C) N 187.9 Iso, where N_x is now known to be N_F. Initially labeled N_S, the discussion about the nomenclature is left for Sec. VI B. The associated enthalpy of the N-N_F transition is in this case also very small $0.2\,\mathrm{kJ\,mol^{-1}}$, comparable with that of N_S-N_F measured for DIO. Similar values are reported for RM734 homologues [16,74]. Recently, by means of precision adiabatic scanning calorimetry, Thoen *et al.* [75] have shown that the N-N_F transition in RM734 is close to a tricritical point.

Despite coming from different molecular families, Chen *et al.* [76] have recently shown that DIO and RM734 show complete miscibility. All the mixtures show Iso, N, and N_F phases. Such results importantly demonstrate that the low-temperature phases of both materials are the same phase. The reported mixtures also show the appearance of the N_S phase for DIO concentrations >50%. For intermediate concentrations, the poor compatibility of the crystal phases of both materials results in the suppression of the crystallization and the stabilization of the ferroelectric nematic phase at lower temperatures.

1. X-ray scattering and birefringence

In either case, DIO or RM734, x-ray experiments [15,16,77] show only diffuse scattering at both small and wide angles, and thus, the presence of long-range translational order was ruled out, and the mesophases were assigned an N-like character. Additionally, a couple of distinctive characteristics of the x-ray behavior have been highlighted in the case of RM734, with respect to classical NLCs [16]. In either of the fluid phases, the scattering intensity is extremely weak, requiring long exposure times to obtain good signal-to-noise ratios. Additionally, in both nematic phases (N and N_F), diffuse peaks (002, 003) are seen at small angles parallel to the external aligning field, i.e., along the director, Fig. 2(c). Such observations have also been reported for different members of the RM734 family, all of them exhibiting the N_F phase [17,71]. Similar features have also been described for DIO [76]. Interestingly, for an RM734 homolog material in which the nitro group is replaced by a nitrile group (RM734-CN, which uniquely exhibits N phase), none of these behaviors is observed [71,77]. As will be discussed below in the MD simulation section, such additional small-angle scattering peaks seem to be the result of polar ordering in the polar state [71].

Orientational order parameters $\langle P_2\rangle$, $\langle P_4\rangle$, $\langle P_6\rangle$, and $\langle P_8\rangle$ have been extracted from small- and wide-angle x-ray scattering measurements for RM734 and show a discontinuous increase at the N-N_F transition, while $\langle P_{10}\rangle$ is effectively zero at any temperature [see Fig. 2(e)] [77]. The increase of orientational order at the transition is also evidenced in the birefringence. Measurements of Δn for both materials show similar temperature behavior, with an increasing value of Δn while decreasing temperature in the N phase. The N-N_F transition is then characterized by the jump of Δn (see Fig. 2(g), Fig. S17 in Ref. [20], or Fig. 3(a) for an RM734 fluorinated homolog in Ref. [74]). Such a sudden increase is not observed for DIO at the N-N_S transition, where only a change in the slope is observed for Δn, as shown by Brown *et al.* [74].

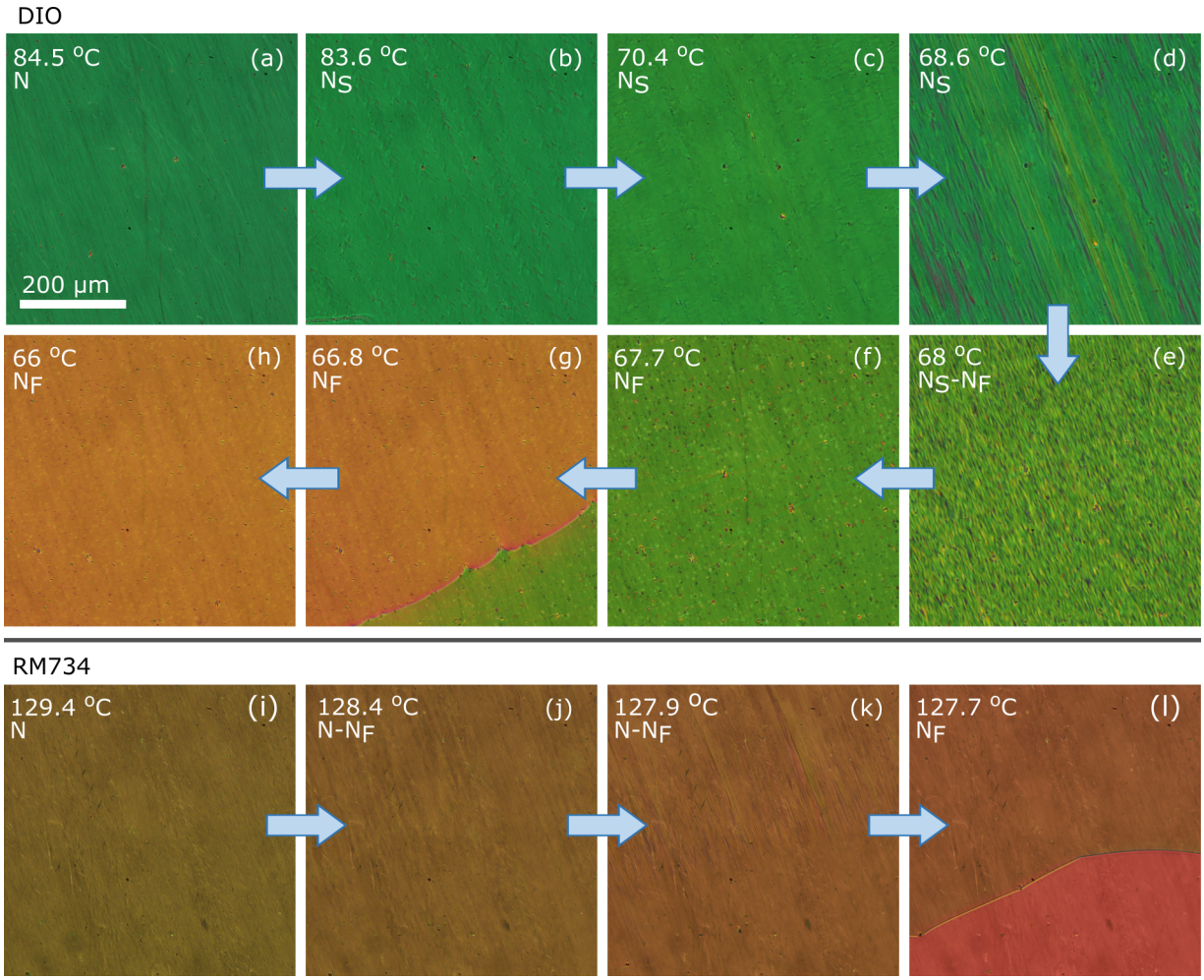

FIG. 7. Polarizing optical microscopy images of the textures of (a)–(h) DIO and (i)–(l) RM734 on cooling through the N-N_S-N_F and N-N_F phase sequences, respectively. Images taken in EHC 8 μm planar cells with antiparallel rubbing. Image width 540 μm.

A jump in the birefringence is then observed at the N_S-N_F transition.

2. *Transitions by polarizing optical microscopy*

Optical texture changes over the transitions have been extensively described for RM734 [18–20,78,79] and DIO [15,69,74,76]. For the latter, the N- N_S transition is characterized by increased pretransitional nematic flickering, directly related to the fluctuations of the nematic director. At the transition, freezing of the strong fluctuating mode takes place, which is observed as a wavefront propagating throughout the cell, as also pointed out by Brown *et al.* [74], see Supplemental Movie 1 [80]. Textures of N and N_S are similar, with that of the latter characterized by strongly reduced flickering and by the appearance of zigzag defects (in cells with planar alignment, see Fig. 7) which slowly disappear on further cooling. Transition to the N_F phase is then marked by the strong destabilization of the uniform texture in the form of stripes, which at a slightly lower temperature disappear and lead to a homogeneous texture equivalent to that in the N phase. This transition is also accompanied by material flow. It should be noted here that, as will be covered below in Sec. V A, the nature of the confining surfaces (alignment layer, rubbing, and pretilt) exerts a strong influence on the final observed structure [78,79,81]. In very similar terms, in the case of RM734 (Fig. 7), the transition has been described to show strong pretransitional behavior in the N phase characterized by strong fluctuations followed by the freezing of the nematic flickering and immediately followed by destabilization of the homogenous orientation of the director, characterized by a striped texture [18,19,78]. This destabilization leads to the recovery of a homogeneous texture and with it the flickering. Transition on slow cooling can be found in Supplemental Movie 2 [80]. Comparing both materials and the description of the transitions, it can be conjectured that the narrow temperature range in which RM734 shows freezing of the nematic fluctuations indeed resembles a very narrow N_S phase followed by a transition to the N_F phase. We will return to this discussion in Sec. VI B.

3. *Pretransitional behavior:* $\mathbf{K_1}$ *and* $\boldsymbol{\Delta\varepsilon}$

Studies of the director orientational fluctuations close to the phase transition in RM734 by Mertelj *et al.* [18] and Mandle *et al.* [71] show that the observed strong pretransitional fluctuations in the N phase are a consequence of the strong softening of the splay elastic constant K_1. Here, K_1 is

unusually low in the studied temperature range and decreases toward zero when approaching the transition [see Fig. 2(a)]. Decreasing K_1 has been also observed for DIO and several mixtures in the proximity of N-N_S transition [76,82]. Interestingly, a comparison with RM734-CN shows that, in the absence of the polar nematic phases, the K_1 value remains small, but the softening of the pretransition behavior is absent [71].

Such pretransitional behavior is also reflected in the dielectric properties of RM734 in the preceding N phase. Measurements of the parallel component of the dielectric spectra for RM734 have been reported for a broad frequency range by Sebastián *et al.* [19]. The spectrum in the N phase is characterized by the presence of two low-frequency relaxation modes (low frequency as lower frequency than in the isotropic phase), instead of the single relaxation found in classical nematic phases corresponding to the molecular reorientation around the long molecular axis (see Fig. 3 in Ref. [19]). Of both, that of lower frequency shows strong softening on approaching the N-N_F transition, characterized by the fast decrease of its frequency, deviating from Arrhenius behavior, and the divergence of its amplitude, reaching values up to $\Delta\varepsilon_{low} \sim 6000$ [Fig. 2(a)]. Together with the behavior of the splay elastic constant, it shows that the transition between nematic phases in RM734 is a ferroelectric-ferroelastic phase transition. As shown in Sec. II B 3, the measured splay elastic constant is indeed an effective elastic constant, smaller than the bare K_1 by the term $-\gamma^2\varepsilon_0\Delta\varepsilon_{low}$. For an increasing electric susceptibility, at a given temperature, the effective elastic constant will become zero, and the uniform nematic phase will become unstable toward splay deformation. Such linear dependency between the effective elastic constant and the electric susceptibility is nicely reproduced by the experimental data [Fig. 2(b)].

4. Dielectric measurements

Dielectric measurements in the ferroelectric phase must be taken with caution. Accurate measurements require successful aligning strategies, and as shown in Sec. V, it is a challenging task in the case of the N_F phase. For example, while in the N phase, either some conventional homeotropic aligning agents or bare metallic electrodes seem to succeed in inducing homeotropic alignment. No homeotropic alignment was achieved in the ferroelectric state.

In either case, giant values (∼10 000) of the dielectric permittivity have been reported for RM734 in the N_F phase (see Fig. S5 in Ref. [69]). The situation can be compared with the dielectric measurements for DIO reported by Nishikawa *et al.* [15] and Brown *et al.* [74]. In this case, dielectric spectra in the N phase have been reported to be characterized by a single active relaxation process, whose amplitude, although large for standard nematics, increases only to values ∼200 (see Fig. 4(e) in Ref. [74]). The transition to the N_S (addressed as N_x in Ref. [74]) phase results in the initial decrease in the amplitude, followed by a sharp diverging increase as the polar correlations grow. In the N_S phase, an additional high-frequency relaxation appears, which again disappears in the N_F phase, which is characterized by a very strong relaxation process with a frequency of 2 kHz [74]. From the behavior of relaxation modes under bias fields, Brown *et al.* [74] consider two scenarios: one in which local ferroelectric and antiferroelectric fluctuations coexist in the N_S phase and another in which the phase presents some polar order but with an additional director modulation in the nanometer range, which results in the additional high-frequency mode.

In either case, remarkably large dielectric permittivity values, of the order of 10 000 have been reported in the N_F phase for RM734, DIO, or comparable materials [15,69,74].

5. Polarization measurements

Such unprecedented values of the dielectric permittivity indicate the existence of large polar ordering in the N_F phase. Polarization measurements have been performed via the standard triangular/square-wave method in which the field-induced polarization reversal current is measured. Despite the different approaches, i.e., use of in-plane or out-of-plane application of driving fields, reported polarization values saturate at remarkable values of the order of several microcoulombs per square centimeter: 6 $\mu C/cm^2$ for RM734 [20,76] [see Fig. 2(d)], 2.5–6 $\mu C/cm^2$ for DIO [15,74,76], or 6–7 $\mu C/cm^2$ (∼2 $\mu C/cm^2$ in case of planar cells with out-of-plane field) for an homologous of RM734 [83]. In RM734 and DIO mixtures, the polarization saturation value varies continuously from one material to the other [76]. The reported polarization values are of the same order as those found for polar columnar phases [66] but an order of magnitude larger than common values found for classical ferroelectric phases [84] or bent-core polar phases [61].

6. Second harmonic generation

Further evidence of the strong polar character of N_F is the extraordinary second harmonic generation (SHG) properties reported so far. Values of NLO coefficients ranging between 1 and 10 pm V^{-1} have been reported for a wide number of materials from the RM734 (material 1a) and DIO (material 5b) families, comparable with several ferroelectric solid materials (see comparison table S4 of the supporting information of Ref. [69]). Recent SHG measurements of RM734 give a d_{333} coefficient of 5.6 pm V^{-1} [85]. As pointed out by Folcia *et al.* [85], this value is one of the largest NLO coefficients reported for a ferroelectric liquid crystal (FLC) despite the molecules not being specifically designed for NLO applications.

The temperature dependence of SHG intensity for DIO shows that, in the absence of applied field, SHG intensity only appears in the N_F phase (see Fig. 8). However, under the application of small electric fields, the N_S phase also becomes SHG active [15]. The same trend is observed for materials investigated by Li *et al.* [69], where SHG activity strongly increases in the N_F phase in the absence of external fields. According to their results, the SHG signal increases over a wide range of temperatures around the transition, with a marked pretransitional behavior.

The strong SHG activity has led to the implementation of SHG microscopy studies. The RM734 N-N_F transition has been studied via SHG microscopy (Fig. 2 in Ref. [19] and see Figs. 9 and SI.14 by Sebastián *et al.* [78]), showing that on cooling from the N phase, the first detected SHG image corresponds to the stripe destabilization sequence at the transition described before, with a periodicity of a few microns. Further

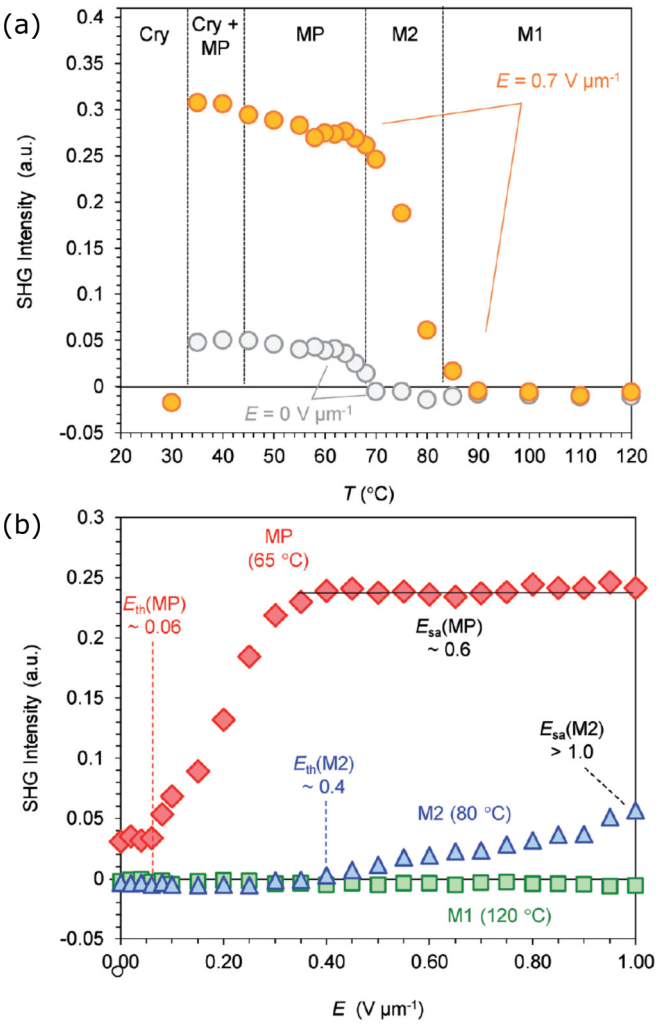

FIG. 8. (a) Temperature dependence of the second harmonic generation (SHG) signal of DIO for *p-p* polarization. (b) Field dependence of the SHG signal of DIO at three temperatures in the N (M1), N_S (M2), and N_F (MP) phases. © 2017 WILEY-VCH Verlag GmbH & Co. KGaA, Weinheim. Reprinted with permission from Ref. [15].

cooling leads to the homogenization of the SHG texture, with a dependence on the direction of the incoming polarization well described by $\cos^4\phi$, where ϕ is the angle between the incoming polarization and the cell rubbing direction. Also, by means of SHG interferometry, it was determined that adjacent bands in the N_F texture of RM734 correspond to opposite polarizations (Fig. S8 in Ref. [69]).

7. Direct isotropic to ferroelectric nematic transition

Notably, several materials have been found that exhibit a direct Iso-N_F transition [67,72,74]. Materials showing such behavior span from monomeric compounds [67,74] to main-chain LC polymers [72]. In this case, the transition is characterized by a stronger enthalpy change (reported values for different materials are between 5.2 and 10 J/g) and exhibits some distinct characteristics.

Independently, Manabe *et al.* [67] and Li *et al.* [72] have shown that, on cooling from the Iso phase, the transition into

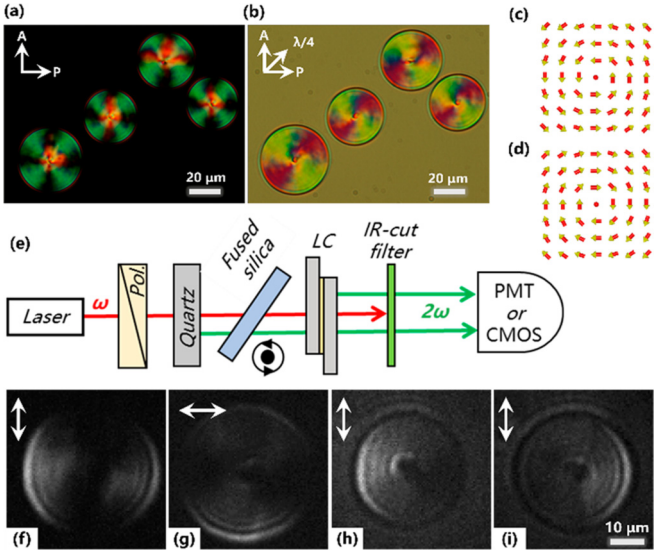

FIG. 9. (a) and (b) Polarizing optical microscopy (POM) images of domain nucleation on the direct Iso-N_F transition. (c) and (d) Tangential anticlockwise and clockwise nematic director arrangement. (e) Second harmonic generation (SHG) and SHG-interferometry setups. (f) and (g) SHG microscopy images and (h) and (i) SHG-interferometry images for two complementary interferometry conditions. © 2021, American Chemical Society. Reprinted with permission from Ref. [72].

the N_F phase occurs via nucleation of spherical domains (see Fig. 3 in Ref. [67] and Fig. 9 here). Such domains steadily grow on further cooling and eventually begin to coalesce and fill the whole area in a mosaiclike pattern made of domains divided by disclination lines, generally oriented along the rubbing direction. This process takes place over several degrees, e.g., 5 °C for material Nt4, picked as a representative example of the main-chain oligomers/polymers [72]. By means of SHG microscopy and interferometric microscopy, Li *et al.* [72] show that, in the circular domains, the nematic director forms a +1 defect with a concentric pattern, for which clockwise and anticlockwise directions of polarization can be found with equal probability. At lower temperatures, the mosaic texture is revealed to consist of polar domains with the alternating direction of polarization. Interestingly, longer oligomers/polymers show larger SHG intensity, varying between 50 and 150 times the SHG intensity of Y-cut quartz.

As before, the polar nature of the phase is also reflected in the dielectric properties. When cooling from the isotropic phase, dielectric permittivity grows from values ∼100 in the isotropic phase to values up to, for example, 20 000 in the case of a monomeric material [67] and in the range of 1000–10 000 for the oligomers/polymers [72]. In the latter case, reported polarization values are in the range of 1.5 $\mu C/cm^2$, slightly lower than those for the monomeric materials.

B. Chiral phases

Also remarkable, despite the early stages of the field, is the simultaneous realization of polar cholesteric phase N_F^* [86–88]. Two different approaches have been described. Nishikawa *et al.* [86] and Feng *et al.* [87] reported on the chiral

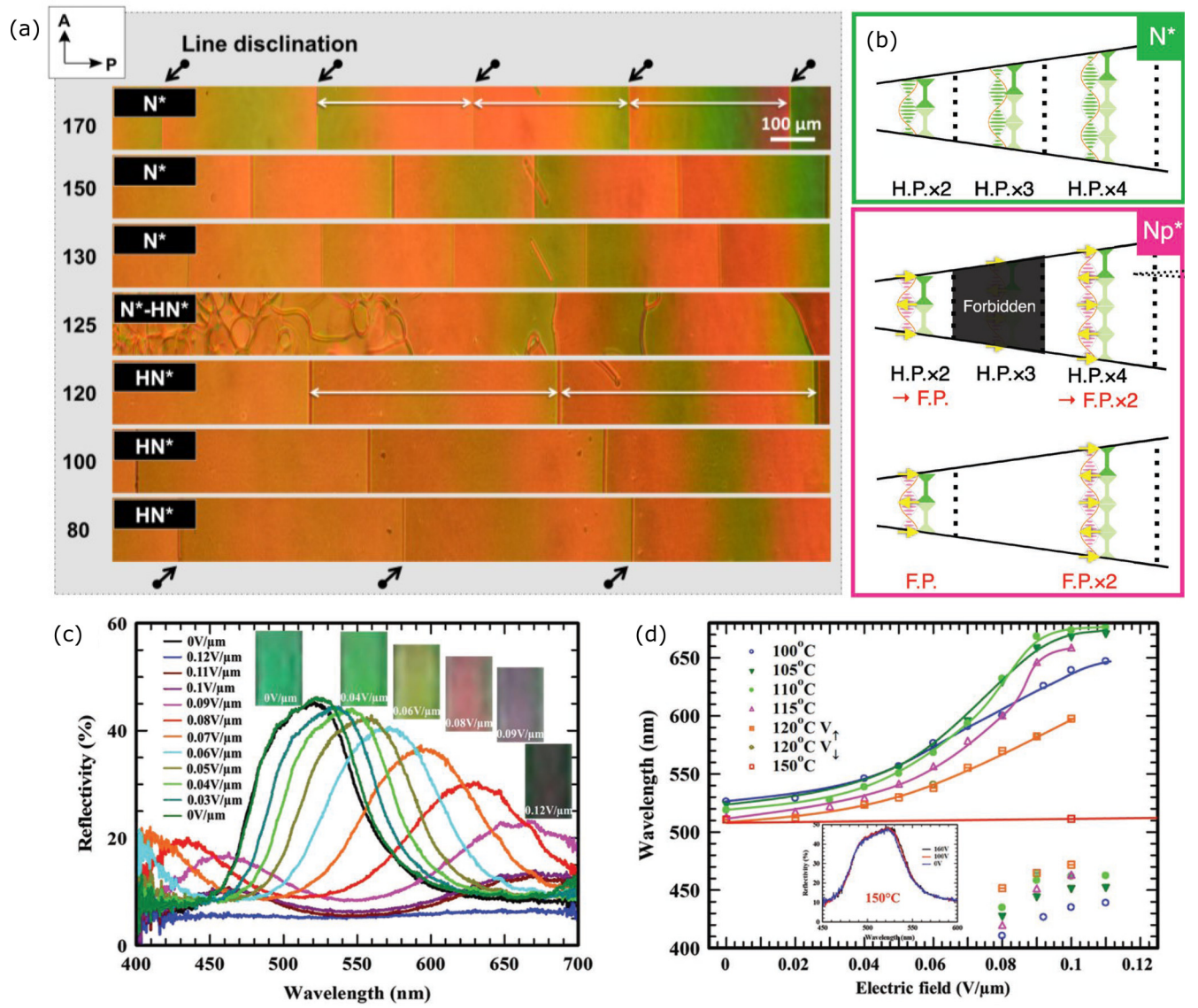

FIG. 10. (a) Doubling of length between Grandjean-Cano lines in a wedge cell for RM734 doped with a RM734 chiral generator analogue. © 2021 Published under PNAS license. Reprinted with permission from Ref. [89]. (b) Schematic illustration of the proposed helical structures in wedge cells for N* and N_F^* phases. © 2021 Wiley- VCH GmbH. Reprinted with permission from Ref. [87]. (c) Selective reflection for a RM734 + 2% BDH1281 mixture for different applied fields and (d) its voltage dependence at different temperatures. © 2021 Wiley- VCH GmbH. Reprinted with permission from Ref. [88].

ferroelectric nematic phase by doping DIO and RM734, respectively, with commercially available dopants. Meanwhile, Zhao *et al.* [88] doped RM734 with chiral generators, synthesized by introducing chiral groups at different positions of RM734. In either case, all the doped systems show a high-temperature N* phase followed by the polar counterpart, in which the polarization as well as the nematic director twist along the helical axis (see Fig. 1).

In all cases, helical pitch smoothly varies with temperature, without drastic changes in the N*-N_F^* transition. Investigation of the pitch length via the conventional Grandjean-Cano method shows interesting behavior of the Grandjean-Cano lines. In conventional N* materials, the distance between Grandjean steps (L) is determined by the helical pitch (p) by the relationship $L = p/(2\tan\theta)$, where θ is the angle of the wedge cell. It should be noted here that, depending on the Burgers vector, L can be twice as large [89]. Nevertheless, it has been observed that, at the N*-N_F^* transition, edge dislocation lines rearrange, and the distance between them doubles [see Fig. 10(a)]. The underlying mechanism for such an effect, far from being related to a drastic doubling of the helical pitch, has been attributed to the polarization direction at the surfaces. While in the N* phase half-pitch structures are allowed, in polar N_F^*, even multiples of the half-pitch are needed to maintain the polarization in the same direction along the surface avoiding additional defects. Thus, in N_F^*, it is proposed that the following relationship is valid $L = p/(\tan\theta)$ [86,88] [Fig. 10(b)]. Additionally, the coupling between the helical structure and the polarization results in enhanced control of the tunability of selective reflection of visible light.

Fields as low as 0.02–0.1 V/μm are reported to be enough for reversible tuning [87] [see Fig. 10(c)]. Also, enhanced performance is reported in terms of switching times for optical transmittance, with 10–90% on and off times of the order of 250 μs, respectively, with a reduction for the off time to 15 μs in the case of using a reverse pulse field [86].

To conclude this section, it should be mentioned that, in addition to the described phase sequences, two additional polar phases have been reported for an RM734 analogue, with the addition of a fluorine group in the center benzene ring by Saha *et al.* [83] following the phase sequence on cooling Iso-N-N_F-F_2-F_3. Such a phase sequence was determined via DSC measurements combined with spontaneous polarization measurements. Although the material is the same as compound 2 reported in Ref. [74] and the difference could arise from different purities, such results highlight the possibility of discovering additional polar phases in the present context.

C. MD simulations

Computer simulations play an important role in the understanding of the formation of liquid crystalline phases and their properties [90,91]. Immense progress in computer power and advanced force field models enabled all atomistic MD simulations of various LC phases. As the formation of orientational order in a liquid is a many-body problem, which is difficult to address with theory, the MD simulations give insight into dynamics and correlations between the molecules which are a consequence of many-body interactions.

The material RM734 was studied by two independent MD simulations by Chen *et al.* [20] and Mandle *et al.* [71]. The simulations differ in the choice of force fields (in Ref. [20] APPLE&P [92,93], in Ref. [71] GAFF-LCFF [94,95]), the number of molecules per simulation (368 in Ref. [20] vs 680 in Ref. [71]), and production MD simulation length (∼20 ns in Ref. [20] vs 250 ns Ref. [71]). Both simulations failed to observe the transition between the apolar nematic to polar nematic state, so the simulation of either polar or apolar state was determined by the starting configuration. Both simulations of the polar state of RM734 gave comparable values of the order parameters S, $\langle P_1 \rangle$ and the spontaneous polarization and similar positional correlations showing stronger polar head-to-tail pairing in the polar than in the apolar simulation (Fig. 11). The position of the x-ray scattering peaks calculated from the polar MD simulation by Mandle *et al.* [71] matched well the positions of the measured low angle peaks [Figs. 2(c) and 6 in Ref. [71]), while those from apolar did not, which supports the relevance of MD simulations. As the low angle peaks are experimentally observed also in the nonpolar nematic phase well above the phase transition temperature to the polar phase, this indicates that strong polar correlations are present already there. These observations suggest that small-angle x-ray scattering could be a useful probe of polar order within apolar and polar NLC.

The differences between the positional correlations in the polar and apolar states on their own do not explain why in a particular material the polar state is more favorable than the apolar. However, in the simulations in Ref. [71], a notable difference between the states was observed in the density and mobility of the molecules. In those simulations, the density was ∼0.5% larger, and the diffusion of the molecules was faster in the polar than in the apolar state [Fig. 11(d)]. The increase of the density was also confirmed experimentally for RM734 [Fig. 2(f)], as well as for a fluorinated homologue [83]. On the contrary, in the material RM734-CN, which is very similar to RM734 but does not exhibit a polar phase, the simulation showed that the polar and apolar states have the same density, while the diffusion is slower in the polar state. This indicates that, in the materials exhibiting the polar phase such as RM734, the molecules can pack better, and simultaneously, they are more mobile when in the polar state, which suggests that the polar phase is more favorable than the apolar from the point of view of the excluded volume. These observations were confirmed by simulations of several other materials from the RM734 family [71] and for DIO [96].

V. ANCHORING AND ELECTROOPTICS

The switching behavior of any LC is strongly affected by the confining surfaces. In the case of ferroelectric nematic phases, the interaction with the surfaces is additionally complex due to electrostatic effects.

A. Surfaces and anchoring effects

The importance of the confining boundaries was systematically studied by Caimi *et al.* [81], where the alignment and structures induced by different alignment surfaces were explored and surfaces assessed by their degree of coupling strength and anchoring orientation. It is evidenced that the textures and defect structures, together with the field response, are strongly dependent on the surface treatment.

While silane-coated surfaces are usually employed in thermotropic nematics to achieve homeotropic alignment, they induce planar alignment in the case of the N phase of RM734, homogeneous when rubbed [81]. In the N_F phase, both rubbed silanized and rubbed Teflon surfaces show strong quadrupolar orientational coupling with the RM734 molecules and to a less extent polar coupling (with the direction of polarity antiparallel to the rubbing direction), resulting in homogeneous areas of planar alignment in which embedded twisted domains can be observed. The latter correspond to areas in which one of the surface polarities is reversed. From the different aligning strategies, only bare hydroxylated glass resulted in homeotropic alignment in the N phase, which turns into inhomogeneous planar alignment in the N_F phase.

Homeotropic alignment in the N phase was also reported for DIO and RM734 for two different cells: treated with octadecyltrimethoxysilane from EHC Japan [15] and with bare ITO electrodes [19]. In both cases, transition to the N_S or N_F phase was accompanied by the development of a sandy/grainy texture with no clear extinction position [15,19].

Commercially available LC cells for planar alignment most commonly employ rubbed polyimide layers with a small pretilt, necessary for defect-free alignment. While pretilt results in equivalent surface energies for $\mathbf{n}$ and $-\mathbf{n}$, it also results in nonzero polar surface energy, differentiating between $\mathbf{P}$ and $-\mathbf{P}$ states as pointed out by Chen *et al.* [79]. Cells can be assembled with surfaces having parallel or antiparallel rubbing directions, which has been shown to result in different textural

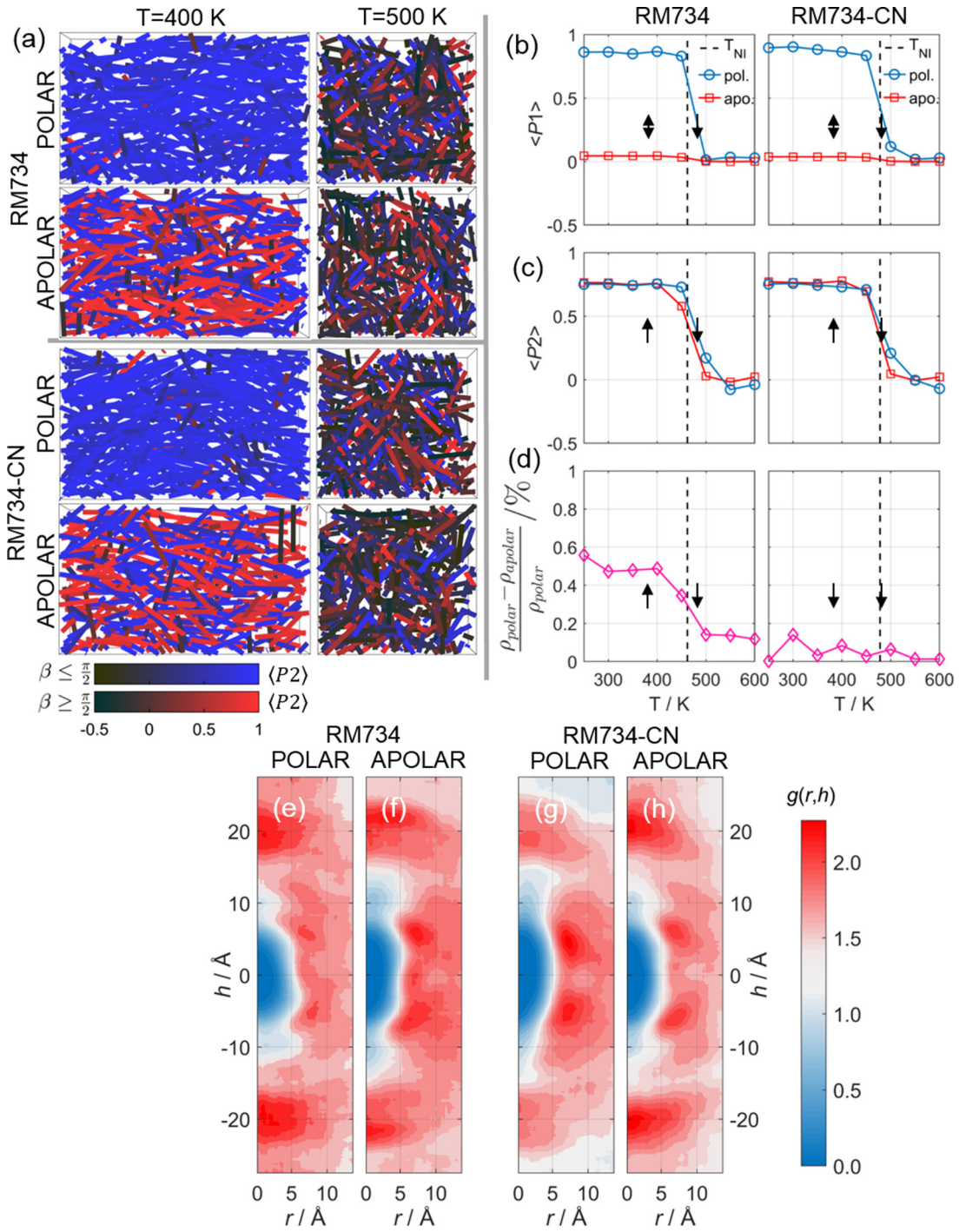

FIG. 11. (a) Molecular dynamics simulations snapshots in polar and apolar configurations of RM734 and RM734-CN at two temperatures, 400 and 500 K. Dependence of the order parameters (b) P1 and (c) P2 on the simulation temperature for both materials in both polar and apolar configurations. (d) Difference in the simulated mean density between polar and apolar configurations. (e)–(h) Cylindrical pair-correlation functions as obtained for both materials and polar and apolar configurations at 400 K. Reproduced from Ref. [71], licensed under CC BY 4.0.

characteristics (Figs. 12 and 13). In either case, strong planar alignment is observed in the N phase. In the N_F phase, parallel rubbing would orient the polarization in the same direction on both surfaces, resulting in a monodomain uniformly aligned sample (see Fig. 13 and Figs. 2(f)–2(i) in Ref. [79]). On the other hand, in antiparallel rubbed cells, in-plane polar orientation at both surfaces with opposite directions is expected. When cooling from the N phase (see description of the transition in previous sections), initially the N_F phase is characterized by a homogeneous texture, appearing right after the stripe destabilization (see Supplemental Movies 1 and 2 [80]). At a lower temperature (very close to the transition in the case of RM734 and a few degrees after in the case of DIO), a wall front propagates through the cell, usually initiating at some

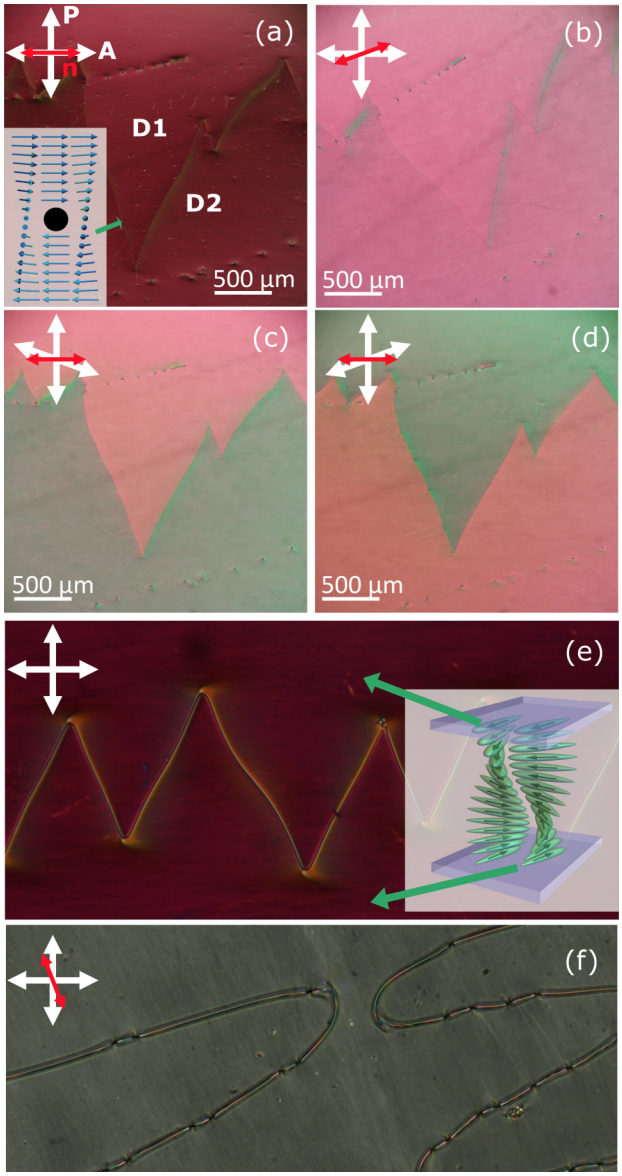

FIG. 12. (a)–(d) π-twist domains of opposite handedness in the N_F phase of RM734 in extinction position, with the sample rotated and on uncrossing analyzer clockwise and anticlockwise. (e) Detail of sierra-shape wall. (a)–(e) Reproduced from [78], published under CC BY-NC-ND 4.0. (f) Pointlike structures decorating walls. Reproduced from [18], licensed under CC BY 4.0.

surface defects. When two of the fronts come together, they can either annihilate or give rise to a 2π wall dividing domains with opposite twist handedness [78,79]. When those walls are perpendicular to the rubbing direction, they stretch over long distances undeformed. However, when directed along the rubbing direction they adopt a sierra-shaped configuration, with the wall bending at angles between 50° and 70° (Fig. 12), as shown by Sebastián *et al.* [78]. Uncrossing of the polarizers reveals opposite optical behavior in both domains, characteristic of twisted domains with opposite handedness [74,78,79] [Figs. 12(c) and 12(d)]. In such domains, polarization rotates a π turn in either the left- or right-handedness direction. The simplest of the twist structures is a linear π twist across the

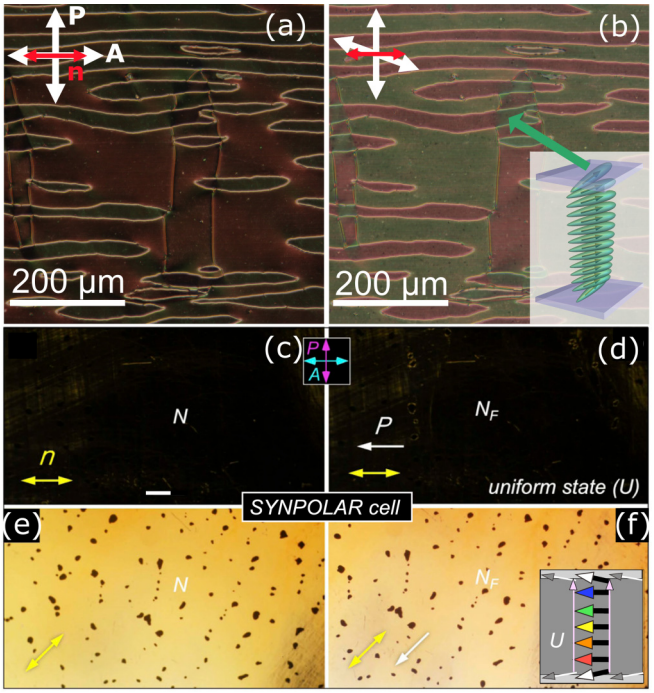

FIG. 13. (a) and (b) Simple twist structures surrounded by domain walls pinned at the surface. Reproduced from [78], published under CC BY-NC-ND 4.0. (c)–(f) Textures of the N and N_F phase in a SYNPOLAR cell (parallel rubbed cells). Reproduced from [79], published under CC BY-NC-ND 4.0.

cell thickness, although the symmetry of the dependence of the relaxation rates of the director fluctuations on the wave vector, reflecting the symmetry of the structure, points toward more complicated structures [78]. Nevertheless, these twisted domains can span up to several millimeters, and a single domain can even extend over a whole cell on some occasions. Depending on the antiparallel cell type and surface conditions, it is also possible to observe some additional elongated domains embedded in the pi-twist domains [78]. They are characterized by bright domain walls, pinned in the surface and their optical behaviour indicates the presence of a simple twist as shown in Figs. 13(a)–13(b).

Additionally, textures in cells with surfaces characterized by bidirectional rubbing have also been studied by Chen *et al.* [79]. Bidirectional rubbing results in nonpretilted surfaces, with a preferential parallel orientation of **n** along the rubbing but no in-plane polarity. In the N_F phase, both directions of polarization are then equally probable, and the texture is characterized by domains of opposite polarization direction [79].

B. Electro-optic behavior

Electro-optics in LCs is of utmost relevance, as it constitutes the basis of their technological potential. In the polar nematic phases, unique features are to be expected. However, is to be noted that electro-optic behavior will strongly depend on the confining boundaries determining the corresponding director structure and on the direction of field application.

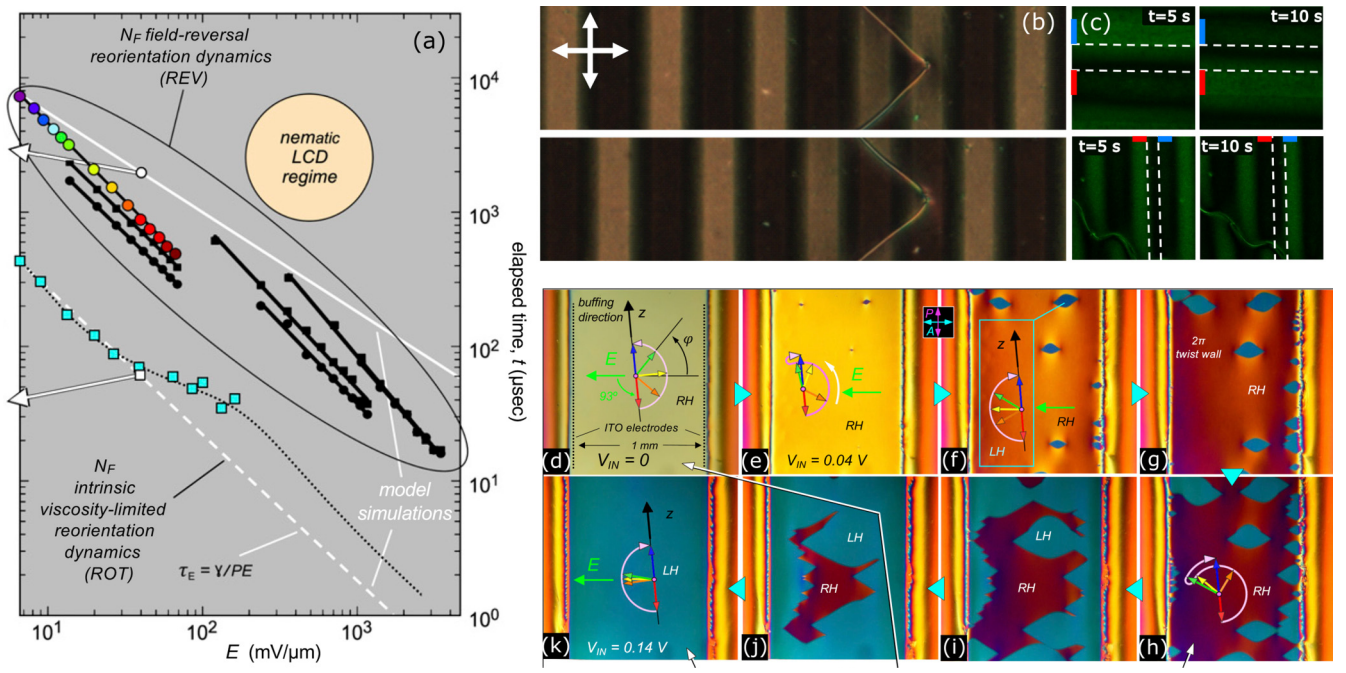

FIG. 14. (a) Experimental and simulated reorientation times for the polarization reversal and viscosity-limited electro-optic modes. Reproduced from [79], published under CC BY-NC-ND 4.0. (b) and (c) Electrooptic response [polarizing optical microscopy (POM) and second harmonic generation (SHG)] of two adjacent π-twist domains in an IPS cell with rubbing direction parallel to electrodes. Reproduced from [78], published under CC BY-NC-ND 4.0. (d)–(h) Domain-mediated polarization reversal of RM734. Reproduced from [79], published under CC BY-NC-ND 4.0.

Considering out-of-plane fields applied in planarly aligned cells, it has been shown that, due to its large value, reorientation and deformation of polarization results in an induced charge that neutralizes the applied field hindering the reorientation (see Sec. II B 4). This results in very large voltages needed for splay-bend reorientation of the director when compared with the standard N phase (see sec. VI, supporting information in Ref. [20]). However, interesting behavior can still be observed at lower voltages [78]. In antiparallel planar rubbed cells, where cells are covered by π-twist polar domains, the application of smaller fields (low-frequency AC fields of amplitude $\sim$0.3 V/μm) causes the deformation of the domain wall, enhancing the sierra-shaped configuration of those running parallel to the rubbing direction or triggering the growth of new line defects that eventually open and result in new domains. For applied voltages oscillating between 0 and V, it can be seen how domains of one handedness progressively grow, while the opposite domains shrink. Reversal of field polarity ($-$V to 0) consistently reverses the process.

The richness of polarization-director structures is also reflected in the electro-optic behavior upon application of in-plane fields. In the predominant π-twist domains, Chen *et al.* [79] have described three distinct electro-optic modes. The application of an electric field perpendicular to the rubbing direction in the surfaces (i.e., the field is perpendicular to the director in the surfaces but parallel to **n** in the center of the cell) reorients the molecules, squeezes the twist to the cell surfaces [78,79], and gives rise to a quasiuniform state. This reorientation is shown to be fast, with a characteristic time scaling of $\tau = \gamma/PE$, resulting in $\sim$100 ms for fields of $\sim$10 mV/μm [79] [Fig. 14(a)]. In commercial IPS cells, with interdigitated electrodes, such a mode results in opposite switching characteristics for adjacent electrode gaps and mirrored across the domain walls dividing domains of opposite handedness [78] [Fig. 14(b)]. While short pulses minimize the effect of mobile charges, application of slower alternating fields shows bimodal response, as ionic impurities have time to redistribute, screening the field and the polarization charges.

If the in-plane field is applied opposite to the polarization in the quasiuniform state induced by the field in the previous case, the response starts in the twisted areas close to the surface and propagates through the cell as solitons in the polarization field until creating a twisted region in the center of the cell [79]. Such a reorientation is much slower than the previous molecular reorientation and scales with the applied field also as $\tau \propto 1/E$ [79]. Additionally, a third mode has been described, like the observations for out-of-plane fields, consisting of the nucleation of domains with more favorable twist handedness depending on the field polarity (Fig. 14(c) reproduced from Fig. 4 in Ref. [79]) and their propagation throughout the cell. The monodomain is maintained after the field removal, resulting in bistable switching between domains of opposite handedness.

VI. EXPERIMENTAL CHALLENGES

In this section, several experimental techniques relevant to the present field are introduced. The different challenging aspects of such measurements are outlined together with the consideration of currently absent studies.

A. Materials

One of the first steps for the development of the field relies on the ability to develop materials exhibiting the ferroelectric nematic phase. As evidenced by the time that has passed from the prediction to the experimental realization, this is indeed not a straightforward task. Systematic studies have shown that small molecular variations can suppress the N_F phase [69,70]. For example, Mandle *et al.* [70] have shown that a large dipole moment or polarizability is not sufficient for the appearance of the polar phase, and the removal of a single ester unit or lateral chain implies the disappearance of the phase. The strong potential for the applicability of polar nematic phases in technological solutions relies on the ability to synthesize materials exhibiting the ferroelectric phase at broad temperature ranges around room temperature. A few examples are close to it [67,72] and constitute a very promising starting point. There is a compelling need to extend and deepen the knowledge about which fundamental features of molecular design are required for the promotion of polar nematic phases. As further discussed below, MD simulations might have an important role in this task. It should be noted here that, during the writing of this Perspective, materials have been reported [97] exhibiting ferroelectric nematic phases, evidencing the velocity at which the field is evolving. Promising progress has been done in recent years, and we believe that the field will advance fast with the development of materials and probably, more importantly, mixtures with improved applicability.

B. Polarizing optical microscopy and anchoring effects

One standard method for the imaging of optically anisotropic materials is polarizing optical microscopy (POM), in which the sample is placed in the optical pathway between polarizers. In the standard configuration, the polarizers are kept orthogonal. When propagating through the sample, the incident linearly polarized light splits into two perpendicular components, travelling within the sample at different velocities. The properties of elliptically polarized transmitted light are determined by the second polarizer − analyzer. In the case of LCs, this analysis provides information on the underlying director structure [98].

For this purpose, LCs are typically studied under confinement in thin cells, in which the boundary conditions (for example, chemical, steric, or dipolar interactions) at the surface determine the orientation of the molecules at the interface, which for thin samples is kept via elastic forces across the cell [99]. As covered in Sec. V A, surface and anchoring effects in the N_F phase are not only determined by the orientational coupling in the surface but also by the polar coupling. This leads to different orientations and confined structures than in the classical nematic phase for standard aligning techniques. A strong tendency for the appearance of twisted structures is also evidenced. Obtaining a detailed analysis of the underlying structure from the interpretation of POM images of inhomogeneous birefringent media is complicated. Provided the structure is known or can be modeled, one can always rely on excellent numerical tools that have been developed to calculate POM images of arbitrary director structures [100,101]. That is, it requires the knowledge of the structure to simulate POM images that will match the experiment and does not work vice versa in complex cases, where the exact structure cannot be deduced from the POM experiments. This is especially the case when complicated twisted structures are involved, as POM experiments only give integrated information across the cell thickness. Thus, the development of an adequate theory for the N_F phase (Sec. VII C) is of utmost importance.

LC phases typically exhibit distinct optical textures such as domains and defect structures that enable their differentiation using POM. Distinctive anchoring of the N_F phase offers direct ways of its identification. In Fig. 12, typical defect structures observed in N_F are shown. The most characteristic are the sierra-shaped walls that appear in thin antiparallel rubbed cells and separate the π-twisted domains with opposite handedness. In thicker cells (depending on the material, typically $>10\,\mu$m), these walls are more curved and are typically decorated by pointlike structures. They are also less stable, they tend to annihilate, and often, after the relaxation, a whole cell consists of a single π domain. In a thick cell, such domains may show good extinction between crossed polarizers because of the guiding of optical polarization, so one should be careful not to interpret such domains as uniform. An additional method for identification of the N_F phase via microscopy observations has been proposed by Rudquist [102] using a hybrid planar cell with a uniformly rubbed surface on the bottom and a circularly rubbed pattern on the top one.

One should also note here that strong memory effects can be observed in the cells reported in Sec. V after several heating and cooling runs, strongly affecting the resulting textures. The large polarity of the N_F phase could be held responsible for such an effect, rewriting the initial polarity of the aligning layer. Additionally, although uniformly aligned samples can be obtained in some cases, appearance of unintentional surface imperfections can be triggered by surface imperfections. This brings us to one of the important challenges to be faced. Currently, a bottleneck for the characterization of the phase and its exploitation is our ability to control the alignment and structures in the N_F phase. This applies for simple uniform planar or homeotropic structures, which are critical for the determination of some material parameters, such as NLO coefficients, dielectric constants, or polarization values, or for more complicated structures, for which precise control of the orientation of the director would also lead to the control of the orientation of the polarization, and thus tailored polarization structures. Compared with solid ferroelectrics, polarization, in this case, can vary continuously in space.

C. SHG

Optical studies of the response of the material to an electric field can infer ferroelectric order, but their drawback is that assumptions about the structure and its field response must be made. Thus, they alone cannot be used to unambiguously prove that the phase is ferroelectric. For that, SHG studies and/or measurements of the hysteresis loop are needed [103]. In this respect, SHG is an essential tool for assessing the structural polarity of materials, as only those lacking the center of inversion symmetry allow SHG to appear.

SHG is a nonlinear optical process, in which a photon with frequency 2ω is generated in a material via the absorption of two photons of frequency ω, i.e., frequency-doubled light emerges from a material pumped by a laser beam. Such a process is coherent, and in the case of molecular systems, it is determined by the orientational average of the molecular third rank hyperpolarizability tensor. In comparison with electric measurements, the advantage of SHG is that it is a noninvasive optical method, which detects polar order also in the absence of an external field, and therefore, ionic impurities do not affect the measurements. By using the SHG interferometry option, the method is also sensitive to the sign of **P** (e.g., see Fig. 9). Combining the investigations of field responses with SHG measurements also gives information on induced polarization (e.g., see Fig. 8), which is in electrical measurements often obscured by ion contributions.

Combined SHG microscopy and interferometry are called for as essential and of great interest in the case of polar nematic phases. Not only will it bring valuable information for the development of the theory on electric polarization orientation but also for future design and exploitation of the SHG capabilities of the materials. As mentioned above, the calculation of light propagation in nonhomogenous birefringent media is complex and requires numerical methods. The analysis and calculation of the generation and propagation of SHG light in such structures additionally get difficult, as coherent effects need to be considered. Currently, there are no appropriate numerical tools for such studies, and they need to be developed.

Such progress will also be remarkably useful in terms of electro-optic behavior studies. The electro-optic behavior described in Sec. V B is expected to be more broadly and deeply analyzed with the development of materials. The large polarization values result not only in complex linear electrooptic behavior but also entail the corresponding second harmonic electro-optic switching, as demonstrated in Ref. [78] [Fig. 14(b)]. This is expected to be the subject of many future studies.

D. Dielectric characterization

Broadband dielectric spectroscopy is an exceptionally useful experimental technique for the investigation of LC phases and phase transitions, in which measurement of noncollective and collective orientational polarization contributions to the dielectric spectra allows us to study the dynamics of the material [104]. Nonpolar nematic phases are characterized by two molecular modes of orientational polarization, i.e., molecular rotation around the long and short molecular axes, contributing differently to the parallel and perpendicular components of the macroscopic dielectric permittivity. In the present case, broadband dielectric spectroscopy measurements through the nonpolar nematic and different polar nematic phases are of utmost interest. As has been shown in Sec. III, the onset of collective behavior can be well found in the nonpolar nematic phase (whose dielectric behavior greatly differs from that of classical nematics). Detailed studies and comparison between different materials will allow studying the development of spontaneous polarization through the phase transitions and should shed light onto which molecular correlations are determinant for the development of one or another phase sequence. Such a comparison together with studies of thickness dependence effects is currently missing but needed.

Proper characterization of the parallel and perpendicular components requires successful aligning strategies, which as discussed above remains a challenge. In this context, it is important to remark that, as pointed out by Brown *et al.* [74], while the effect of the thin aligning layers of the measuring cells in the measured values can be disregarded for conventional LCs, that is not the case for the present ferroelectric materials, which can lead to considerably different values. Additionally, the very small values of the splay elastic constant result in considerably low threshold voltages for Fredericks transition in the high-temperature N phase already far from the transition. On lowering the temperature, V_{th} is further decreased. Thus, typical probe voltages (0.1–0.5 V_{rms}) can fall above V_{th}, leading to field-induced changes in orientation during the measurements. Consequently, it is important to pay attention to this detail, considering that adequate reduced voltages of $\sim$20 mV_{rms} can also lead to noisy signals. For the appropriate understanding of the molecular polar correlations, the careful measurement of the broadband spectra, its analysis, and the identification of the relaxation modes are necessary. Finally, such careful analysis and interpretation should identify the modes associated with the reorientation of large polarization values that can lead to misinterpretation of ε values [105]. Due to all of this, to the difficulties in achieving homeotropic alignments, the different geometries, or substrates used by different research groups and to the presence of free charges, the interpretation of the absolute permittivity values and comparisons between materials should be considered very carefully.

E. Polarization measurements

For the determination of spontaneous polarization (P_S) in liquid crystalline samples, the triangular (square)-wave method is broadly used, in which P_S is determined from the analysis of transient currents under triangular(square) AC voltages [106]. Determination of P_S requires the accurate deconvolution of the different conductive, capacitive, and polarization terms. While triangular fields result in a linear capacitive current contribution, such a contribution in the case of square voltage is often more complicated than a single exponential, which could lead to overestimation of the polarization value. Additionally, there are several limitations to the technique. Election of wave amplitude and frequency is also determinant in these experiments, where the measuring frequency should be lower than the inverse of the polarization relaxation time but large enough to avoid effects produced by charges. Application of large voltages can lead in this case to turbulent flow, which will also contribute to the transient currents. The high polarity of the sample additionally imposes some limitations. As pointed out in Ref. [83], difference between polarization values obtained for in-plane and out-of-plane cell geometries (see Sec. IV A 5) is a consequence of the large internal electric field that needs to be surpassed to rotate the polarization out-of-plane, which can lead to underestimated values for out-of-plane geometries. On the other

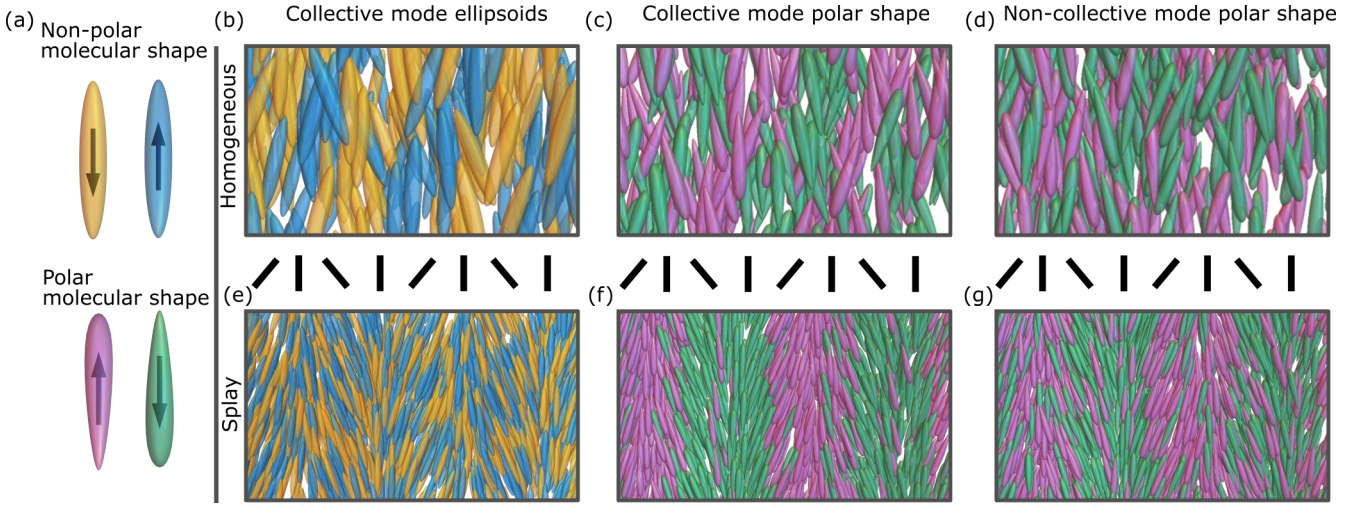

FIG. 15. Fluctuation modes (a) Color code for different up-down orientations of molecular constituents having head-tail symmetry (blue-yellow ellipsoids) and lacking head-tail symmetry, i.e., polar-shaped (wedge shaped pink-green). Collective mode for (b) nonpolar-shaped and (c) polar-shaped molecules. (d) Without collective mode (no polar correlations) for polar-shaped molecules. Splay fluctuations of (e) nonpolar-shaped molecules showing no coupling of splay and polarization, while the flexoelectric polarization is (f) enhanced in the presence compared with (g) the absence of collective polarization mode.

hand, nonuniformity of the field in the case of in-plane cells, for which the electrode does not extend all the thickness, can lead to nonaccurate determination of the area, leading to nonaccurate values of the polarization. Because samples with homogeneously aligned polarization in the absence of the field are very difficult to achieve, determination of the value of the spontaneous polarization, that is, polarization in the absence of the field, is challenging. This poses a problem in the temperature interval where the polarization value changes significantly and the polarization value is a nonlinear function of the applied field.

VII. FUNDAMENTAL CHALLENGES AND FUTURE DEVELOPMENTS

In this section, several important fundamental open questions are presented. One of the very important questions that should be addressed in future years is the mechanism by which polar ordering originates in these phases. In this respect, some thoughts and contributions are collected here for consideration. Strong pretransitional behavior, as discussed above, carries information of the physical mechanisms that drive the phase transitions. Interpretations of the differences in the pretranstional behavior, which lead to either the N_F or N_S phase, is a challenge we comment on first. It is followed by some remarks on currently observed phase sequences, pointing out the challenge of demonstrating the uniformity of the polar ground state, fundamental for the adequate identification of the polar phases. There is also a place for a short discussion about phase nomenclature, regarded as necessary at this stage. Also of utmost importance is that the understanding of these phases; description of their properties; and prediction of structures, defects, or field responses requires development of a suitable theoretical model, which is currently not available. This is a critical challenge, which is here just outlined with some aspects that should be important to consider. Development of the experimental aspects of this field will be strongly intertwined with the development of a suitable theory. Finally, success in both experimental and fundamental understanding of these materials will determine their future applicability. Here, as a short recap, we have collected several thoughts on applicability of polar nematic phases into technological solutions based on some contributions that outline remarkable exploitable properties.

A. Pretransitional behavior: The role of the splay in the phase transitions

1. Pretransitional behavior

The transition from N to N_F phase has been shown to be a ferroelectric-ferroelastic transition in which the growth of ferroelectric order is accompanied by the softening of the splay orientational elastic constant [18,19]. The orientational fluctuations of **n** are characteristics of the nematic phase, and because the NLCs are optically uniaxial with the optical axis parallel to **n**, these fluctuations manifest optically as distinctive nematic flickering. In a bulk NLC, their eigenmodes are overdamped plane waves with two branches: splay-bend and twist-bend [38]. Relevant to our discussion are the pure splay modes schematically shown in [Figs. 15(e)–15(g)]. If the shape of the constituents lacks head-tail symmetry, the splay fluctuations cause that, locally, more constituents are oriented in the same direction [Fig. 15(f)]. If they also carry longitudinal dipole moments, this ordering will result in local electric polarization. This is a well-known flexoelectric effect [45]. On the other hand, for some reason, e.g., steric and/or electrostatic interaction, the polar order of several neighboring molecules may become favorable, which manifests as a collective mode observed in dielectric spectra. This mode can be described as fluctuations in the magnitude of the polarization [Figs. 15(b) and 15(c)]. By flexoelectric coupling, required by symmetry, this mode is coupled to splay fluctuations, so instead of independent polarization and splay mode, there are two coupled modes. One is primarily the splay mode, seen optically; the

other is primarily the polarization mode observed by dielectric spectroscopy. Because of the coupling, splay fluctuations promote the growth of the polarization [Fig. 15(e)], and vice versa, polarization fluctuations promote splay, which results in softening of the effective splay elastic constant. This seems to be the driving for the transition from the nematic to the polar nematic state. It also explains why, in MD simulations, the transition between nematic and polar nematic is not observed because, due to small size and periodic boundary conditions, the splay fluctuations are prevented. As shown in Sec. II B 3, this mechanism predicts the appearance of the 1D or 2D modulated antiferroelectric splay nematic phase N_S as an intermediate phase between N and N_F [18,19,28]. The models that use the lowest order coupling terms in the free energy [Eqs. (8) and (9)] predict the second-order phase transition with the modulation wave vector growing from zero at the N-N_S phase transition. By adding higher-order coupling (gradient) terms, the N-N_S transitions can become (weakly) first order with the finite modulation wave vector at the phase transition.

The study and comparison of pretransitional behavior for materials with different phase sequences or temperature ranges of intermediate N_S phase should lead to discerning the mechanisms responsible for a given phase sequence and the origins of the phase polarity.

2. Phase sequences

As will be discussed in the paragraph below, in the case of DIO, the phase, which appears in between N and N_F, has indeed been identified by Chen *et al.* [107] as modulated splayed phase. This leaves us with the question of whether the phases in RM734 also follow the same sequence. In our publications [18,19], the transition was identified as N-N_S, guided by the unambiguous role of the K_1 softening in the transition and appearance of a stripped polar structure observable by SHG microscopy in a narrow temperature region of a few tenths of a degree before undergoing the transition to what is now known as N_F phase. Recent precision adiabatic scanning calorimetry measurements by Thoen *et al.* [75] show a very weakly first-order transition, where pretransitional variations are significantly larger in the higher-temperature phase. Optically, the transition from N to N_S phase would be characterized by the freezing of the splay fluctuations. Optical observations under slow cooling (see Supplemental Movie 2 [80]) show for RM734 a narrow but discernible temperature range in which splay fluctuations are frozen, in between the N phase and the low-temperature phase. Such a texture is compatible with the N_S phase observed in DIO. This raises the question of whether the transition is a direct N-N_F transition or N-N_S-N_F double transition, maybe in the case of the confined sample, stabilized due to surface effects. Additionally, ionic impurities could play an important role in the stabilization of a narrow N_S phase. This will be, for sure, the focus of future research.

On the other hand, the question of whether the experimentally observed N_F phase is indeed uniform remains open. In comparison with the nonpolar nematic phase, in which the uniform state is easily achieved in planar or homeotropic cells, this is not the case in the N_F phase. There, under confinement and different aligning strategies, the director structure shows a strong tendency to twist and to form topological line/wall defects. These may be the consequences of surface and electrostatic effects. However, one should bear in mind that, in the N_F phase, due to the symmetry, in the elastic free energy, linear terms in deformation are allowed which might destabilize the uniform alignment [7]. In this regard, proving the uniformity of the ground state is challenging, as experimentally accessible N_F structures will always be affected by surface and electrostatic effects.

Finally, given that we are currently at the early stages of the research in ferroelectric nematic materials, it cannot be ruled out that the progressive development of materials, from monomers to polymers, will lead to the discovery of additional phases.

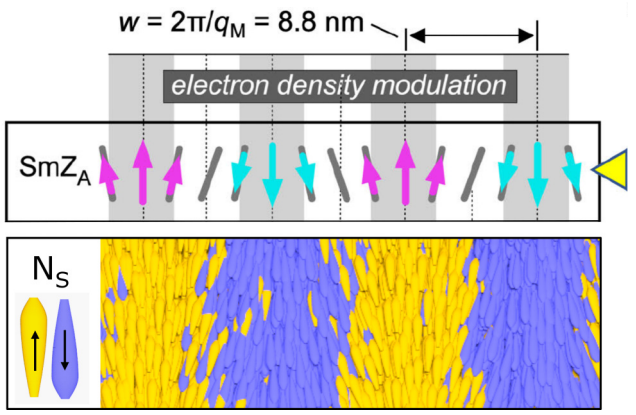

FIG. 16. (top) Schematic representation of the proposed SmZ_A structure, where gray shadowed areas have a different density than the layer boundaries (white shadowed areas). Reproduced from Ref. [108], licensed under CC BY 4.0. (bottom) Schematic representation of the splay nematic phase N_S.

3. Intermediate phase and nomenclature

In a recent preprint [107], the intermediate phase in DIO has been shown to exhibit periodic modulation of density in the direction perpendicular to **n** with the periodicity of 8.8 nm. Chen *et al.* [107] propose the structure of the phase being layered antiferroelectrically, with the nematic director and polarization oriented parallel to layer planes and the polarization alternating in sign from layer to layer accompanied by alternating splay (Fig. 16, top). They named the phase SmZ_A. The proposed structure is identical to the splay nematic phase N_S (Fig. 16, bottom), although the authors of Ref. [107] did not make that connection. Considering that the density depends on the degree of polar order, as demonstrated by Mandle *et al.* [71] via MD simulations, it is expected that the N_S phase exhibits density modulation. No doubt, the naming of the phase will be a subject of future debates. In our opinion, there are two arguments to consider. First, the N_S phase, as shown in Sec. II B, in its origin belongs to the family of modulated nematic phases such as the N_{TB} and N_{SB} phases. It is important to note that density modulation is also expected for N_{SB}. The modulated N_S phase, as schematically shown in Fig. 16, is predicted by the theory of several authors [18,28,52], where periodicity of the modulation depends on the material parameters. Additionally, the intermediate phase in DIO appears to

have a modulation period ∼40 times larger than the molecular width, while thermotropic smectic phases typically exhibit a modulation period of the order of the molecular size. With this in mind, we believe that, to avoid confusion and misinterpretation, the phase should be considered in the family of modulated nematic phases and thus named splay nematic phase N_S.

B. The origin of polar order

Berardi *et al.* [11] showed that polar shape with nonequal head-tail interactions can lead to polar nematic phase and that additional electric dipolar interaction disrupts the polar order. Thus, the obvious question is whether polar order arises primarily because of the shape or because of the electrostatic interaction. As mentioned in Sec. II, in the case of dipolar interaction, the positional correlations of nearest neighbors strongly affect polar ordering. The question is: What positional correlations promote polar order. To answer this, instead of looking at what positional correlations will lead to polar order, we may look at the positional correlation caused by polar order. These can be found in a study of ferrofluids made of spherical nanoparticles with large enough magnetic dipole moment in an external magnetic field [108]. In that study, it has been shown that, due to dipolar interaction, a pseudocrystalline lamellar hexagonal particle arrangement is formed in which particles are arranged in hexagonal planes so that the distance between them is ∼2 particle diameters, and their magnetic dipole moments lay in the plane of the layer [Fig. 17(a)]. This arrangement is very similar to what was proposed by Madhusudana [109] to explain the mechanism for polar order in ferroelectric NLCs. He showed that, at high enough density, the polar arrangement of elongated constituents with continuously alternating positive and negative charges (which roughly correspond to a line of dipoles with centers separated by twice the dipole size) becomes energetically more favorable than nonpolar arrangement. In the polar state, the neighbors are positionally shifted along the long axis to minimize electrostatic energy [Fig. 17(b)]. This electrostatic interaction is very short ranged, so it acts only between the nearest neighbors, and as such, it is obviously different from the one proposed by Born [6]. This mechanism of polar order relies on rather strong positional correlations, which is likely to cause a decrease in molecular mobility. This raises the question of whether such a phase will remain a nematic liquid, or will it crystalize? In RM734, a nonpolar crystalline phase is thermodynamically more stable than the polar nematic phase, and in a crystal, a shifted polar packing motive of the nearest neighbors is observed, although the overall order is nonpolar [18]. On the other hand, the experiments showing that oligomers made of repeating units carrying a dipole form the polar nematic phase [72] support the idea that periodic charge modulation of the constituents promotes polar order.

The question of the origin of polar order remains open. While the (attractive) interactions between molecules are important, one must bear in mind that the system must remain in a liquid state. This happens when the entropic contributions to the free energy prevail over the attractive interactions. As discussed in Sec. IV C, MD studies showed that, in materials exhibiting the polar nematic phase, the molecules in the polar

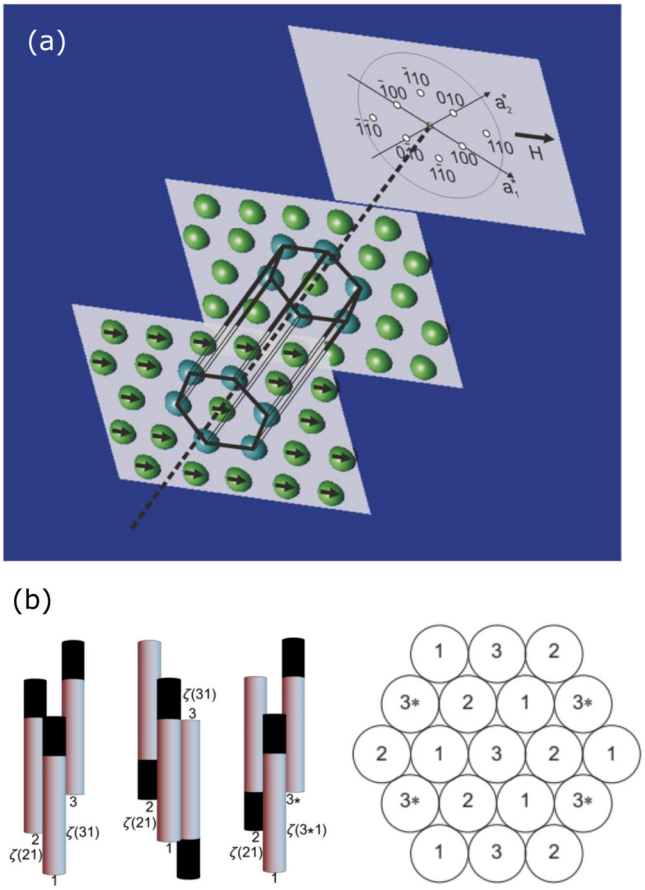

FIG. 17. (a) Schematic representation of a hexagonal arrangement for magnetic spherical particles. ©2003 American Physical Society. Reprinted with permission from Ref. [109]. (b) Scheme of polar rod-triplets and their proposed arrangement. © 2021 American Physical Society. Reprinted with permission from Ref. [110].

phase are more densely packed and, at the same time, more mobile than in the apolar nematic phase, which shows that the polar phase is more favorable from the excluded volume point of view. This demonstrated that the MD studies can be a very useful tool in predicting the existence of the polar nematic phase and supporting the material design. However, simulating the phase transition from apolar to polar nematic phase remains a major challenge for future MD studies. A particular challenge is to incorporate splay deformation in the MD simulation box and check the hypothesis that the splay deformation promotes the polar order and causes the phase transition. The in-depth analysis of the orientational and positional ordering of molecules in MD simulations may also give information on the average potential felt by a molecule and shed light onto how a subtle interplay between polar shape (steric interaction) and weak short-range electrostatic interactions leads to polar order in a liquid.

C. Development of the theory

The structure, field response, and the defects in the nonpolar, achiral, or chiral nematic phase are successfully modeled and predicted by LdG tensor theory or, when the scalar order parameter can be assumed constant, by Oseen-Frank theory.

It is a wish and a challenge to establish a similarly successful model to describe and predict the structure, defects, and field response of the ferroelectric nematic phase. This phase is more complicated than apolar nematic because it has lower symmetry, and consequently, more terms are allowed in the free energy, among them terms linear in deformation. Which of them are relevant is a question for future investigations combining experiments and modeling. Additionally, because the electric polarization values are large, the theory needs to include electrostatics. As discussed in Sec. V and references therein, while in the apolar nematic the surface anchoring can be relatively simply described, the interaction of N_F with the surface is far more complex and sensitive to details, such as pretilt, the position of electrodes, and whether they are grounded or floating, the presence of charged impurities, etc. The appropriate description of the surface interaction is a crucial part of the model.

In most of the materials exhibiting the N_F phase, the direction of the dipole and molecular long axis are not parallel, and consequently, a polar biaxial phase may form. This interesting but very complex case was systematically studied by Longa and Trebin [110]. They described the system with coupled biaxial tensor order parameter and polarization, and by using symmetry considerations, they showed that three different biaxial polar phases can exist, one of them chiral. In that study, they demonstrate the complexity with which theoretical description is faced, and on the other hand, it poses a challenge for experimentalists to look for possible other polar nematic phases.

D. Applications

The final question is the applicability of ferroelectric NLCs. This question is, of course, highly correlated with the development of materials with a suitable temperature range of the N_F phase. However, there is no doubt that these materials will have significant impact on technological implementation of LCs. Although their importance spans from chemistry and biology to physics, in the discussion here, we will focus only on the potential of the physical characteristics in terms of technological applications of the N_F materials. As for the display applications, this question pertains to whether the N_F materials can surpass the performance of the apolar NLCs in terms of speed and voltages needed for optical switching. While the switching of the N_F was shown that it could be of the order of 10–100 μs, using fields 10^5–10^6 V/m [79], the real performance study of the optical response of material on the pixel size, achieving similar intensity (or phase) contrast, as in the case of conventional NLCs, is still missing. In our opinion, the N_F materials may be also interesting for nondisplay applications. As discussed in Sec. IV A, the N_F materials exhibit nonlinear optic coefficients comparable with those of solid nonlinear optical materials, and provided that in the future we will learn to control the structures and domains in the N_F phase, they could be used in tunable nonlinear optical components. A remarkable property of N_F materials is their huge temperature-dependent dielectric permittivity. Araoka *et al.* [111], for example, demonstrated that large changes in the dielectric permittivity through the phase transition from N_S to the N_F phase can also be achieved by phototuning and how such behavior can be exploited in electronic applications. It has also been shown that confinement in silanized glass microchannels, either straight or including bend sections, results in continuous N_F order and thus **P** order along the channel axis [112]. Such a finding by Caimi *et al.* [112] opens the door for the exploration of the use of N_F phases on nonlinear fiber optics elements. Also recently, Máthé *et al.* [113] have demonstrated thermally induced laminar flow in N_F sessile drops, driven by the unique combination of the tangential orientation of polarization, the pyroelectricity of the fluid, and the thermal gradient. Such an effect points toward possible exploitation in thermal energy harvesting. Ferroelectric nematic polymers cannot be so easily switched but are due to large NLO coefficients still interesting for application in nonlinear optics and, as polar materials with large dielectric permittivity, in electronic devices.

Works collected here constitute only the initial stages of research into applications and exploitable properties of these polar nematic phases. It is expected that this field will rapidly grow with the development of materials.

VIII. CONCLUSIONS

The emerging field of ferroelectric NLCs has set in motion very exciting times for soft matter research. In this Perspective, we recapitulated the different theoretical and experimental relevant works that provide the starting framework for future research development. Research on solid ferroelectric materials is vast, and nowadays, they play an important role in numerous everyday devices as well as high technological applications, from piezoelectric sensing and dielectric energy storage to electrocaloric solid-state cooling. Although the idea of a ferroelectric liquid dates to the very beginnings of the discovery of ferroelectricity, 100 years have been needed for their experimental realization. In the liquid ferroelectric state, while retaining mobility typical of a liquid, the molecules spontaneously orient on average in the same direction, which results in the appearance of macroscopic electric polarization. Measured spontaneous polarization values ($\sim 0.05\,\mathrm{C/m^2}$) are comparable with those of some ferroelectric solid materials (e.g., $BaTiO_3$ $0.26\,\mathrm{C/m^2}$ [114]). Very large dielectric susceptibility (of the order of 10 000), outstanding NLO coefficients ($\sim 5\,\mathrm{pm\,V^{-1}}$), and stronger and faster response to electric fields complete the picture. It is the fluid character of the ferroelectric nematic materials that will raise future challenges. Contrary to solid-state ferroelectrics, in an FLC, the polarization can vary continuously in space, and any restructuring will also be accompanied by material flow. Such a key difference speaks, for example, to the possibility of tailored polarization structuring through confining surfaces. Finally, the question remains whether the discovery of the ferroelectric nematic phase will lead to further unambiguous realization of long-searched-for phases as, for example, the biaxial nematic phase, the splay-twist phase, or other polar nematic phases, either predicted, as the 2D splay antiferroelectric phase, or not yet even envisioned. Our success in creating an overarching experimental and theoretical understanding of the already discovered polar nematic phases will play an important role in this subsequent challenge.

Note added. Research of ferroelectric nematic phases is currently very dynamic, and during the editorial processes for the evaluation of this Perspective, several works have been reported, and some of them are listed here. Theoretical approaches for the emergence of modulated nematic phases, including the N_S phase, have been reported by Rosseto and Selinger [115] and Emelyanenko *et al.* [116]. Several materials showing ferroelectric phases have been reported, including highly fluorinated and rigid mesogens by Song *et al.* [117]. Special mention deserves the discovery of ferroelectric smectic A phases reported by Kikuchi *et al.* [118] and in a preprint by Chen *et al.* [119]. Pociecha *et al.* [120] have shown the inversion of the helical twist in materials with intrinsically chiral ferroelectric nematic phase at the N^*-N_F^* transition. Ortega *et al.* [121] have explored the tenability of multiple bandgaps by low electric fields in chiral ferroelectric nematics. Basnet *et al.* [122] investigate polar in-plane surface interactions as sources for domain formation. The behavior of ferroelectric liquid droplets on ferroelectric solid surfaces has been explored by Barboza *et al.* [123].

ACKNOWLEDGMENTS

The authors acknowledge financial support from the Slovenian Research Agency (Research Core Funding No. P1-0192). The authors thank Prof. Satoshi Aya and Prof. Mingjun Huang from South China Advanced Institute for Soft Matter Science and Technology for providing DIO material and Dr. R. J. Mandle from Leeds University for providing RM734 material.

[1] I. Dozov, On the spontaneous symmetry breaking in the mesophases of achiral banana-shaped molecules, Europhys. Lett. **56**, 247 (2001).

[2] R. B. Meyer, Structural problems in liquid crystals, in *Les Houches Summer School in Theoretical Physics, Molecular Fluids*, edited by R. Balian and G. Weill (Gordon and Breach, New York, 1976), pp. 273–373.

[3] M. Cestari, S. Diez-Berart, D. A. Dunmur, A. Ferrarini, M. R. de la Fuente, D. J. B. Jackson, D. O. Lopez, G. R. Luckhurst, M. A. Perez-Jubindo, R. M. Richardson *et al.*, Phase behavior and properties of the liquid-crystal dimer 1″,7″-bis(4-cyanobiphenyl-4′-yl) heptane: A twist-bend nematic liquid crystal, Phys. Rev. E **84**, 031704 (2011).

[4] D. Chen, J. H. Porada, J. B. Hooper, A. Klittnick, Y. Shen, M. R. Tuchband, E. Korblova, D. Bedrov, D. M. Walba, M. A. Glaser *et al.*, Chiral heliconical ground state of nanoscale pitch in a nematic liquid crystal of achiral molecular dimers, Proc. Natl Acad. Sci. USA **110**, 15931 (2013).

[5] V. Borshch, Y.-K. Kim, J. Xiang, M. Gao, A. Jákli, V. P. Panov, J. K. Vij, C. T. Imrie, M. G. Tamba, G. H. Mehl *et al.*, Nematic twist-bend phase with nanoscale modulation of molecular orientation, Nat. Commun. **4**, 2635 (2013).

[6] *Crystals That Flow: Classic Papers from the History of Liquid Crystals*, edited by T. J. Sluckin, D. A. Dunmur, and H. Stegemeyer (CRC Press, Boca Raton, 2004).

[7] F. C. Frank, I. Liquid crystals. On the theory of liquid crystals, Discuss. Faraday Soc. **25**, 19 (1958).

[8] H. Pleiner and H. R. Brand, Spontaneous splay phases in polar nematic liquid crystals, Europhys. Lett. **9**, 243 (1989).

[9] P. Palffy-Muhoray, M. A. Lee, and R. G. Petschek, Ferroelectric Nematic Liquid Crystals: Realizability and Molecular Constraints, Phys. Rev. Lett. **60**, 2303 (1988).

[10] R. Berardi, M. Ricci, and C. Zannoni, Ferroelectric nematic and smectic liquid crystals from tapered molecules, ChemPhysChem **2**, 443 (2001).

[11] R. Berardi, M. Ricci, and C. Zannoni, Ferroelectric and structured phases from polar tapered mesogens, Ferroelectrics **309**, 3 (2004).

[12] T. Watanabe, S. Miyata, T. Furukawa, H. Takezoe, T. Nishi, M. Sone, A. Migita, and J. Watanabe, Nematic liquid crystals with polar ordering formed from simple aromatic polyester, Jpn. J. Appl. Phys. **35**, L505 (1996).

[13] J. Watanabe, L. Yuqing, H. Tuchiya, and H. Takezoe, Polar liquid crystals formed from polar rigid-rod polyester based on hydroxy benzoic acid and hydroxy naphthoic acid, Mol. Cryst. Liq. Cryst. Sci. Technol. A **346**, 9 (2000).

[14] B. Park, Y. Kinoshita, H. Takezoe, and J. Watanabe, Ferroelectricity in the lyotropic cholesteric phase of poly l-glutamate, Jpn. J. Appl. Phys. **37**, L136 (1998).

[15] H. Nishikawa, K. Shiroshita, H. Higuchi, Y. Okumura, Y. Haseba, S. Yamamoto, K. Sago, and H. Kikuchi, A fluid liquid-crystal material with highly polar order, Adv. Mater. **29**, 1702354 (2017).

[16] R. J. Mandle, S. J. Cowling, and J. W. Goodby, Rational design of rod-like liquid crystals exhibiting two nematic phases, Chem. Eur. J. **23**, 14554 (2017).

[17] R. J. Mandle, S. J. Cowling, and J. W. Goodby, A nematic to nematic transformation exhibited by a rod-like liquid crystal, Phys. Chem. Chem. Phys. **19**, 11429 (2017).

[18] A. Mertelj, L. Cmok, N. Sebastián, R. J. Mandle, R. R. Parker, A. C. Whitwood, J. W. Goodby, and M. Čopič, Splay Nematic Phase, Phys. Rev. X **8**, 041025 (2018).

[19] N. Sebastián, L. Cmok, R. J. Mandle, M. R. de la Fuente, I. Drevenšek Olenik, M. Čopič, and A. Mertelj, Ferroelectric-Ferroelastic Phase Transition in a Nematic Liquid Crystal, Phys. Rev. Lett. **124**, 037801 (2020).

[20] X. Chen, E. Korblova, D. Dong, X. Wei, R. Shao, L. Radzihovsky, M. A. Glaser, J. E. Maclennan, D. Bedrov, D. M. Walba *et al.*, First-principles experimental demonstration of ferroelectricity in a thermotropic nematic liquid crystal: polar domains and striking electro-optics, Proc. Natl. Acad. Sci. USA **117**, 14021 (2020).

[21] *Handbook of Liquid Crystals*, edited by J. W. Goodby, P. J. Collings, T. Kato, C. Tschierske, H. Gleeson, and P. Raynes (Wiley-VCH, Weinheim, 2014).

[22] H. Takezoe and A. Eremin, *Bent-Shaped Liquid Crystals: Structures and Physical Properties*, 1st ed. (CRC Press, Boca Raton, 2017).

[23] Y. M. Yevdokimov, V. I. Salyanov, S. V. Semenov, and S. G. Skuridin, *DNA Liquid-Crystalline Dispersions and Nanoconstructions* (CRC Press, Boca Raton, 2011).

[24] P. Oswald and P. Pieranski, *Smectic and Columnar Liquid Crystals: Concepts and Physical Properties Illustrated by Experiments*, 1st ed. (CRC Press, Boca Raton, 2005).

[25] A. Jákli, O. D. Lavrentovich, and J. V. Selinger, Physics of liquid crystals of bent-shaped molecules, Rev. Mod. Phys. **90**, 045004 (2018).
[26] G. R. Luckhurst and T. J. Sluckin, Final remarks, in *Biaxial Nematic Liquid Crystals* (Wiley-Blackwell, Chichester, 2015), pp. 369–374.
[27] M. Lehmann, Low molar mass thermotropic systems, in *Biaxial Nematic Liquid Crystals* (Wiley-Blackwell, Chichester, 2015), pp. 333–367.
[28] M. P. Rosseto and J. V. Selinger, Theory of the splay nematic phase: single versus double splay, Phys. Rev. E **101**, 052707 (2020).
[29] H. Mundoor, S. Park, B. Senyuk, H. H. Wensink, and I. I. Smalyukh, Hybrid molecular-colloidal liquid crystals, Science **360**, 768 (2018).
[30] A. Mertelj, D. Lisjak, M. Drofenik, and M. Copič, Ferromagnetism in suspensions of magnetic platelets in liquid crystal, Nature (London) **504**, 237 (2013).
[31] Q. Liu, P. J. Ackerman, T. C. Lubensky, and I. I. Smalyukh, Biaxial ferromagnetic liquid crystal colloids, Proc. Natl Acad. Sci. USA **113**, 10479 (2016).
[32] H. Mundoor, J.-S. Wu, H. H. Wensink, and I. I. Smalyukh, Thermally reconfigurable monoclinic nematic colloidal fluids, Nature (London) **590**, 268 (2021).
[33] J. V. Selinger, *Introduction to the Theory of Soft Matter: From Ideal Gases to Liquid Crystals*, 2016 ed. (Springer, Cham, Heidelberg, 2016).
[34] R. Rosso, Orientational order parameters in biaxial nematics: polymorphic notation, Liq. Cryst. **34**, 737 (2007).
[35] P. D. Gregorio, E. Frezza, C. Greco, and A. Ferrarini, Density functional theory of nematic elasticity: Softening from the polar order, Soft Matter **12**, 5188 (2016).
[36] B. Huke and M. Lücke, Magnetic properties of colloidal suspensions of interacting magnetic particles, Rep. Prog. Phys. **67**, 1731 (2004).
[37] F. Bisi, A. M. Sonnet, and E. G. Virga, Steric effects in a mean-field model for polar nematic liquid crystals, Phys. Rev. E **82**, 041709 (2010).
[38] P. G. de Gennes and J. Prost, *The Physics of Liquid Crystals*, 2nd ed. (Clarendon Press, Oxford, 1995).
[39] *Soft Matter Physics: An Introduction*, edited by M. Kleman and O. D. Laverntovich (Springer, New York, 2003).
[40] P. M. Chaikin and T. C. Lubensky, *Principles of Condensed Matter Physics* (Cambridge University Press, Cambridge, 1995).
[41] M. Ravnik and S. Žumer, Landau–de Gennes modelling of nematic liquid crystal colloids, Liq. Cryst. **36**, 1201 (2009).
[42] C. W. Oseen, The theory of liquid crystals, Trans. Faraday Soc. **29**, 883 (1933).
[43] D. W. Berreman and S. Meiboom, Tensor representation of Oseen-Frank strain energy in uniaxial cholesterics, Phys. Rev. A **30**, 1955 (1984).
[44] L. Longa, D. Monselesan, and H.-R. Trebin, An extension of the Landau-Ginzburg–de Gennes theory for liquid crystals, Liq. Cryst. **2**, 769 (1987).
[45] R. B. Meyer, Piezoelectric Effects in Liquid Crystals, Phys. Rev. Lett. **22**, 918 (1969).
[46] K. Adlem, M. Čopič, G. R. Luckhurst, A. Mertelj, O. Parri, R. M. Richardson, B. D. Snow, B. A. Timimi, R. P. Tuffin, and D. Wilkes, Chemically induced twist-bend nematic liquid crystals, liquid crystal dimers, and negative elastic constants, Phys. Rev. E **88**, 022503 (2013).
[47] S. M. Shamid, S. Dhakal, and J. V. Selinger, Statistical mechanics of bend flexoelectricity and the twist-bend phase in bent-core liquid crystals, Phys. Rev. E **87**, 052503 (2013).
[48] S. M. Shamid, D. W. Allender, and J. V. Selinger, Predicting a Polar Analog of Chiral Blue Phases in Liquid Crystals, Phys. Rev. Lett. **113**, 237801 (2014).
[49] L. Longa and G. Pająk, Modulated nematic structures induced by chirality and steric polarization, Phys. Rev. E **93**, 040701 (2016).
[50] M. Čopič and A. Mertelj, Q-tensor model of twist-bend and splay nematic phases, Phys. Rev. E **101**, 022704 (2020).
[51] N. Chaturvedi and R. D. Kamien, Mechanisms to splay-bend nematic phases, Phys. Rev. E **100**, 022704 (2019).
[52] E. I. Kats, Stability of the uniform ferroelectric nematic phase, Phys. Rev. E **103**, 012704 (2021).
[53] A. G. Khachaturyan, Development of helical cholesteric structure in a nematic liquid crystal due to the dipole-dipole interaction, J. Phys. Chem. Solids **36**, 1055 (1975).
[54] J. C. Everts and M. Ravnik, Ionically Charged Topological Defects in Nematic Fluids, Phys. Rev. X **11**, 011054 (2021).
[55] J. C. Everts and M. Ravnik, Charge-, salt- and flexoelectricity-driven anchoring effects in nematics, Liq. Cryst. **48**, 423 (2021).
[56] R. B. Meyer, L. Liebert, L. Strzelecki, and P. Keller, Ferroelectric liquid crystals, J. Phys. Lett. **36**, L69 (1975).
[57] R. P. Lemieux, Chirality transfer in ferroelectric liquid crystals, Acc. Chem. Res. **34**, 845 (2001).
[58] Q. Guo, K. Yan, V. Chigrinov, H. Zhao, and M. Tribelsky, Ferroelectric liquid crystals: physics and applications, Crystals **9**, 9 (2019).
[59] J. P. F. Lagerwall and F. Giesselmann, Current topics in smectic liquid crystal research, ChemPhysChem **7**, 20 (2006).
[60] T. Niori, T. Sekine, J. Watanabe, T. Furukawa, and H. Takezoe, Distinct ferroelectric smectic liquid crystals consisting of banana shaped achiral molecules, J. Mater. Chem. **6**, 1231 (1996).
[61] R. A. Reddy and C. Tschierske, Bent-core liquid crystals: polar order, superstructural chirality and spontaneous desymmetrisation in soft matter systems, J. Mater. Chem. **16**, 907 (2006).
[62] A. Eremin and A. Jákli, Polar bent-shape liquid crystals—from molecular bend to layer splay and chirality, Soft Matter **9**, 615 (2012).
[63] D. Miyajima, F. Araoka, H. Takezoe, J. Kim, K. Kato, M. Takata, and T. Aida, Ferroelectric columnar liquid crystal featuring confined polar groups within core-shell architecture, Science **336**, 209 (2012).
[64] J. Guilleme, J. Aragó, E. Ortí, E. Cavero, T. Sierra, J. Ortega, C. L. Folcia, J. Etxebarria, D. González-Rodríguez, and T. Torres, A columnar liquid crystal with permanent polar order, J. Mater. Chem. C **3**, 985 (2015).
[65] A. Akiyama, K. Jido, M. Kohri, T. Taniguchi, and K. Kishikawa, Generation of axially polar ferroelectricity in a columnar liquid crystal phase by introducing chirality, Adv. Electron. Mater. **6**, 2000201 (2020).
[66] H. Takezoe and F. Araoka, Polar columnar liquid crystals, Liq. Cryst. **41**, 393 (2014).

[67] A. Manabe, M. Bremer, and M. Kraska, Ferroelectric nematic phase at and below room temperature, Liq. Cryst. **48**, 1079 (2021).

[68] P. Kirsch, 8—Fluorinated nematic liquid crystals: design, synthesis, and properties, in *Photonic and Electronic Properties of Fluoride Materials*, edited by A. Tressaud and K. Poeppelmeier (Elsevier, Boston, 2016), pp. 159–176.

[69] J. Li, H. Nishikawa, J. Kougo, J. Zhou, S. Dai, W. Tang, X. Zhao, Y. Hisai, M. Huang, and S. Aya, Development of ferroelectric nematic fluids with giant-ε dielectricity and nonlinear optical properties, Sci. Adv. **7**, eabf5047 (2021).

[70] R. J. Mandle, S. J. Cowling, and J. W. Goodby, Structural variants of RM734 in the design of splay nematic materials, Liq. Cryst. **48**, 1780 (2021).

[71] R. J. Mandle, N. Sebastián, J. Martinez-Perdiguero, and A. Mertelj, On the molecular origins of the ferroelectric splay nematic phase, Nat. Commun. **12**, 4962 (2021).

[72] J. Li, R. Xia, H. Xu, J. Yang, X. Zhang, J. Kougo, H. Lei, S. Dai, H. Huang, G. Zhang *et al.*, How far can we push the rigid oligomers/polymers toward ferroelectric nematic liquid crystals? J. Am. Chem. Soc. **143**, 17857 (2021).

[73] S. Dai, J. Li, J. Kougo, H. Lei, S. Aya, and M. Huang, Polar liquid crystalline polymers bearing mesogenic side chains with large dipole moment, Macromolecules **54**, 6045 (2021).

[74] S. Brown, E. Cruickshank, J. M. D. Storey, C. T. Imrie, D. Pociecha, M. Majewska, A. Makal, and E. Gorecka, Multiple polar and non-polar nematic phases, ChemPhysChem **22**, 2506 (2021).

[75] J. Thoen, E. Korblova, D. M. Walba, N. A. Clark, and C. Glorieux, Precision adiabatic scanning calorimetry of a nematic—ferroelectric nematic phase transition, Liq. Cryst. **49**, 780 (2021).

[76] X. Chen, Z. Zhu, M. J. Magrini, E. Korblova, C. S. Park, M. A. Glaser, J. E. Maclennan, D. M. Walba, and N. A. Clark, Ideal mixing of paraelectric and ferroelectric nematic phases in liquid crystals of distinct molecular species, Liq. Cryst. (2022).

[77] R. J. Mandle and A. Mertelj, Orientational order in the splay nematic ground state, Phys. Chem. Chem. Phys. **21**, 18769 (2019).

[78] N. Sebastián, R. J. Mandle, A. Petelin, A. Eremin, and A. Mertelj, Electrooptics of mm-scale polar domains in the ferroelectric nematic phase, Liq. Cryst. **48**, 2055 (2021).

[79] X. Chen, E. Korblova, M. A. Glaser, J. E. Maclennan, D. M. Walba, and N. A. Clark, Polar in-plane surface orientation of a ferroelectric nematic liquid crystal: polar monodomains and twisted state electro-optics, Proc. Natl Acad. Sci. USA **118**, e2104092118 (2021).

[80] See Supplemental Material at http://link.aps.org/supplemental/10.1103/PhysRevE.106.021001 for Supplemental Movies 1 and 2.

[81] F. Caimi, G. Nava, R. Barboza, N. A. Clark, E. Korblova, D. M. Walba, T. Bellini, and L. Lucchetti, Surface alignment of ferroelectric nematic liquid crystals, Soft Matter **17**, 8130 (2021).

[82] N. Sebastián, R. J. Mandle, S. Aya, M. Huang, N. Osterman, M. Lovšin, L. Cmok, A. Petelin, A. Eremin, J. Martinez-Perdiguero, I. Drevenšek-Olenik, M. Čopič, and A. Mertelj, Similarities and differences between two ferroelectric nematic materials (unpublished).

[83] R. Saha, P. Nepal, C. Feng, M. S. Hossain, M. Fukuto, R. Li, J. T. Gleeson, S. Sprunt, R. J. Twieg, and A. Jákli, Multiple ferroelectric nematic phases of a highly polar liquid crystal compound, Liq. Cryst. (2022).

[84] S. Pirkl and M. Glogarova, Ferroelectric liquid crystals with high spontaneous polarization, in *Ferroelectrics—Physical Effects*, edited by M. Lallart (IntechOpen, London, 2011), Chap. 17.

[85] C. L. Folcia, J. Ortega, R. Vidal, T. Sierra, and J. Etxebarria, The ferroelectric nematic phase: an optimum liquid crystal candidate for nonlinear optics, Liq. Cryst. **49**, 899 (2022).

[86] H. Nishikawa and F. Araoka, A new class of chiral nematic phase with helical polar order, Adv. Mater. **33**, 2101305 (2021).

[87] C. Feng, R. Saha, E. Korblova, D. Walba, S. N. Sprunt, and A. Jákli, Electrically tunable reflection color of chiral ferroelectric nematic liquid crystals, Adv. Opt. Mater. **9**, 2101230 (2021).

[88] X. Zhao, J. Zhou, J. Li, J. Kougo, Z. Wan, M. Huang, and S. Aya, Spontaneous helielectric nematic liquid crystals: electric analog to helimagnets, Proc. Natl. Acad. Sci. USA **118**, e2111101118 (2021).

[89] I. I. Smalyukh and O. D. Lavrentovich, Three-dimensional director structures of defects in Grandjean-Cano wedges of cholesteric liquid crystals studied by fluorescence confocal polarizing microscopy, Phys. Rev. E **66**, 051703 (2002).

[90] C. Zannoni, From idealised to predictive models of liquid crystals, Liq. Cryst. **45**, 1880 (2018).

[91] M. P. Allen, Molecular simulation of liquid crystals, Mol. Phys. **117**, 2391 (2019).

[92] O. Borodin, Polarizable force field development and molecular dynamics simulations of ionic liquids, J. Phys. Chem. B **113**, 11463 (2009).

[93] D. Bedrov, J.-P. Piquemal, O. Borodin, A. D. MacKerell, B. Roux, and C. Schröder, Molecular dynamics simulations of ionic liquids and electrolytes using polarizable force fields, Chem. Rev. **119**, 7940 (2019).

[94] J. Wang, R. M. Wolf, J. W. Caldwell, P. A. Kollman, and D. A. Case, Development and testing of a general amber force field, J. Comput. Chem. **25**, 1157 (2004).

[95] N. J. Boyd and M. R. Wilson, Optimization of the GAFF force field to describe liquid crystal molecules: the path to a dramatic improvement in transition temperature predictions, Phys. Chem. Chem. Phys. **17**, 24851 (2015).

[96] R. J. Mandle (private communication).

[97] C. Schilling, P. Nacke, and P. Rybak, Conference report on the 48th German liquid crystal conference, Liq. Cryst. Today **31**, 8 (2022).

[98] T. Lee and I. I. Smalyukh, Conventional and nonlinear optical microscopy of liquid crystal colloids, in *Liquid Crystals with Nano and Microparticles*, edited by J. P. F. Lagerwall and G. Scalia (World Scientific, Singapore, 2016), Vol. 7, Chap. 5, pp. 179–207.

[99] G. Babakhanova and O. D. Lavrentovich, The techniques of surface alignment of liquid crystals, in *Modern Problems of the Physics of Liquid Systems*, edited by L. A. Bulavin and L. Xu (Springer International Publishing, Cham, 2019), pp. 165–197.

[100] A. Petelin, dtmm: diffractive transfer matrix method (IJSComplexMatter, 2021), https://github.com/IJSComplexMatter/dtmm.

[101] G. Poy, Nemaktis (2021), https://github.com/warthan07/Nemaktis.

[102] P. Rudquist, Revealing the polar nature of a ferroelectric nematic by means of circular alignment, Sci. Rep. **11**, 24411 (2021).

[103] H. Takezoe, Polar liquid crystals—ferro, antiferro, banana, and columnar, Mol. Cryst. Liq. Cryst. **646**, 46 (2017).

[104] M. R. de la Fuente and D. Dunmur, Dielectric properties of liquid crystals, in *Handbook of Liquid Crystals*, edited by J. W. Goodby, P. J. Collings, T. Kato, C. Tschierske, H. Gleeson, and P. Raynes (Wiley-VCH, Weinheim, 2014), pp. 1–46.

[105] Y. Shen, T. Gong, R. Shao, E. Korblova, J. E. Maclennan, D. M. Walba, and N. A. Clark, Effective conductivity due to continuous polarization reorientation in fluid ferroelectrics, Phys. Rev. E **84**, 020701 (2011).

[106] K. Miyasato, S. Abe, H. Takezoe, A. Fukuda, and E. Kuze, Direct method with triangular waves for measuring spontaneous polarization in ferroelectric liquid crystals, Jpn. J. Appl. Phys. **22**, L661 (1983).

[107] X. Chen, V. Martinez, E. Korblova, G. Freychet, M. Zhernenkov, M. A. Glaser, C. Wang, C. Zhu, L. Radzihovsky, J. E. Maclennan *et al.*, Antiferroelectric smectic ordering as a prelude to the ferroelectric nematic: Introducing the smectic Z_A phase, arXiv:2112.14222.

[108] A. Wiedenmann, A. Hoell, M. Kammel, and P. Boesecke, Field-induced pseudocrystalline ordering in concentrated ferrofluids, Phys. Rev. E **68**, 031203 (2003).

[109] N. V. Madhusudana, Simple molecular model for ferroelectric nematic liquid crystals exhibited by small rodlike mesogens, Phys. Rev. E **104**, 014704 (2021).

[110] L. Longa and H.-R. Trebin, Spontaneous polarization in chiral biaxial liquid crystals, Phys. Rev. A **42**, 3453 (1990).

[111] H. Nishikawa, K. Sano, and F. Araoka, Anisotropic fluid with phototunable dielectric permittivity, Nat. Commun. **13**, 1142 (2022).

[112] F. Caimi, G. Nava, P. Paiè, R. Osellame, M. A. Glaser, N. A. Clark, E. Korblova, L. Lucchetti, and T. Bellini, Ferroelectric nematics in microchannels: switching and propagation of order (unpublished).

[113] M. T. Máthé, Á. Buka, A. Jákli, and P. Salamon, Ferroelectric nematic liquid crystal thermomotor, Phys. Rev. E **105**, L052701 (2022).

[114] W. J. Merz, Double hysteresis loop of $BaTiO_3$ at the Curie point, Phys. Rev. **91**, 513 (1953).

[115] M. P. Rosseto and J. V. Selinger, Modulated phases of nematic liquid crystals induced by tetrahedral order, Phys. Rev. E **105**, 024708 (2022).

[116] A. V. Emelyanenko, V. Yu. Rudyak, S. A. Shvetsov, F. Araoka, H. Nishikawa, and K. Ishikawa, Emergence of paraelectric, improper antiferroelectric, and proper ferroelectric nematic phases in a liquid crystal composed of polar molecules, Phys. Rev. E **105**, 064701 (2022).

[117] Y. Song, J. Li, R. Xia, H. Xu, X. Zhang, H. Lei, W. Peng, S. Dai, S. Aya, and M. Huang, Development of emergent ferroelectric nematic liquid crystals with highly fluorinated and rigid mesogens, Phys. Chem. Chem. Phys. **24**, 11536 (2022).

[118] H. Kikuchi, H. Matsukizono, K. Iwamatsu, S. Endo, S. Anan, Y. Okumura, Fluid layered ferroelectrics with global $C_{\infty v}$ symmetry, Adv. Sci. 2202048 (2022).

[119] X. Chen, V. Martinez, P. Nacke, E. Korblova, A. Manabe, M. Klasen-Memmer, G. Freychet, M. Zhernenkov, M. A. Glaser, L. Radzihovsky *et al.*, Observation of a uniaxial ferroelectric smectic A phase, arXiv:2206.12965.

[120] D. Pociecha, R. Walker, E. Cruickshank, J. Szydlowska, P. Rybak, A. Makal, J. Matraszek, J. M. Wolska, J. M. D. Storey, C. T. Imrie *et al.*, Intrinsically chiral ferronematic liquid crystals: an inversion of the helical twist sense at the chiral nematic–chiral ferronematic phase transition, J. Mol. Liq. **361**, 119532 (2022).

[121] J. Ortega, C. L. Folcia, J. Etxebarria, and T. Sierra, Ferroelectric chiral nematic liquid crystals: New photonic materials with multiple bandgaps controllable by low electric fields, arXiv:2206.04966.

[122] B. Basnet, M. Rajabi, H. Wang, P. Kumari, K. Thapa, S. Paul, M. O. Lavrentovich, and O. D. Lavrentovich, Soliton walls paired by polar surface interactions in a ferroelectric nematic liquid crystal, Nat. Commun. **13**, 3932 (2022).

[123] R. Barboza, S. Marni, F. Ciciulla, F. A. Mir, G. Nava, F. Caimi, A. Zaltron, N. A. Clark, T. Bellini, and L. Lucchetti, Explosive electrostatic instability of ferroelectric liquid droplets on ferroelectric solid surfaces, Proc. Natl. Acad. Sci. USA **119**, e2207858119 (2022).